AWARD NUMBER:
W81XWH-12-1-0396

TITLE:
Inhibition of Pancreatic Cancer Cell Proliferation by LRH-1 Inhibitors

PRINCIPAL INVESTIGATOR:
Robert J. Fletterick

RECIPIENT:
University of California San Francisco,
San Francisco, CA 94103

REPORT DATE:
December 2014

TYPE OF REPORT:
Final

PREPARED FOR: U.S. Army Medical Research and Materiel Command
Fort Detrick, Maryland 21702-5012

REPORT DOCUMENTATION PAGE

Form Approved
OMB No. 0704-0188

1. REPORT DATE	2. REPORT TYPE	3. DATES COVERED
December 2014	Final	15 Sep 2012 - 14 Sep 2014

4. TITLE AND SUBTITLE
Inhibition of Pancreatic Cancer Cell Proliferation by LRH-1 Inhibitors

5a. CONTRACT NUMBER

5b. GRANT NUMBER
W81XWH-12-1-0396

5c. PROGRAM ELEMENT NUMBER

6. AUTHOR(S)
Robert J. Fletterick

Email: robert.fletterick@ucsf.edu

5d. PROJECT NUMBER

5e. TASK NUMBER

5f. WORK UNIT NUMBER

7. PERFORMING ORGANIZATION NAME(S) AND ADDRESS(ES)
. University of California San Francisco,
San Francisco, CA 94103

8. PERFORMING ORGANIZATION REPORT NUMBER

9. SPONSORING / MONITORING AGENCY NAME(S) AND ADDRESS(ES)
U.S. Army Medical Research and Materiel Command
Fort Detrick, Maryland 21702-5012

10. SPONSOR/MONITOR'S ACRONYM(S)

11. SPONSOR/MONITOR'S REPORT NUMBER(S)

12. DISTRIBUTION / AVAILABILITY STATEMENT
Approved for Public Release; Distribution Unlimited

13. SUPPLEMENTARY NOTES

14. ABSTRACT
We propose to find selective and potent compounds that inhibit activity of the nuclear receptor LRH-1 (Liver Receptor Homolog 1) in human pancreatic cancer cells, blunting their growth, proliferation and spread. Our research is innovative in its approach because the target protein is known to control not just one but multiple regulatory mechanisms essential for tumor growth and spread. Thus by targeting this protein, one might be able to de-activate these mechanisms, inhibiting and even reversing the progression of pancreatic cancer. Conceivably, dietary modifications that affect LRH-1 function may spawn a prophylactic approach to the disease. An additional appeal of LRH-1 as a drug target includes its well-studied ligand-binding pocket, which could be targeted by specific drugs, and the proven efficiency of nuclear receptor inhibitors for treatment of different types of malignancies, including breast and prostate cancers. In this project, we show how to discover selective inhibitors of LRH-1 and analyze them in pancreatic cancer cells. The identified novel inhibitors of LRH-1 could then be developed into a pharmaceutical that will inhibit growth and proliferation of cancer cells in pancreatic tumors, advancing the existing pancreatic cancer therapies.

15. SUBJECT TERMS- nothing listed

16. SECURITY CLASSIFICATION OF:			17. LIMITATION OF ABSTRACT	18. NUMBER OF PAGES	19a. NAME OF RESPONSIBLE PERSON
a. REPORT	b. ABSTRACT	c. THIS PAGE			USAMRMC
U	U	U	UU	32	19b. TELEPHONE NUMBER *(include area code)*

Table of Contents

Page

1. INTRODUCTION:

Preceding research funded by an NIH R21 (2009-2011) grant to the PI demonstrated that aberrant activity of nuclear receptor LRH-1 (Liver Receptor Homologue 1, NR5A2) is associated with pancreatic oncogenesis. Because LRH-1 is pivotal to multiple regulatory pathways essential for tumorigenesis, we hypothesize that this receptor might be a plausible target for pancreatic cancer therapy. Thus, we proposed to find selective antagonists of LRH-1 activity and analyze their effects on pancreatic cancer cell proliferation.

2. KEYWORDS:

Pancreatic cancer, PDAC, nuclear receptor, LRH-1, NR5A2, regulation of transcription, antagonists, small molecule inhibitors, cancer cell proliferation, cell cycle arrest.

3. OVERALL PROJECT SUMMARY:

Aim 1 and **Aim 2** of this program (**Task 1** and **Task 2** of the approved SOW) are completed; substantial progress has been made towards **Aim 3** (**Task 3** of SOW).

Aim 1 (Task 1): Discovery of small molecules – antagonists of nuclear receptor LRH-1.

As proposed in our application, we performed computational filtering of over 5 million compounds and tested top ranked hits in the following biophysical and cell biology assays.

Virtual screening was performed against a constructed model of an inactive state of hLRH-1 LBD, as described in our recently published research article by Benod *et al.* (1). For computational docking experiments, we used a library of 5.2 million commercially available molecules from the ZINC database. Following visual inspection of the resulting top-ranked 500 compounds (~0.01% of the initial library content), twelve molecules were selected for experimental evaluations. From these verification experiments, we identified two compounds - **Cpd 3** (1-(3'-{1-[2-(4-morpholinyl)ethyl]-1H-pyrazol-3-yl}-3-biphenylyl)ethanone; shown docked in the LRH-1 ligand binding pocket in Fig. 1A) and **Cpd 3d2** (4-(3-{1-[2-(dimethylamino)ethyl]-1H-pyrazol-3-yl}phenyl)-N,N,5, 6-tetramethyl-2-pyrimidinamine; shown docked into LRH-1 pocket in Fig. 1B) - that bind to LRH-1 LBD directly. The evidence for direct binding was obtained using two independent methods – *Differential Scanning Fluorimetry* (**Task 1a**) and *Surface Plasmon Resonance* (SPR) using quantitative Biacore based assay (**Task 1b**). Analyses of the SPR response isotherms estimated the corresponding Kd values of 1.5 ± 0.3 μM for Cpd 3 and 1.8 ± 0.4 μM for Cpd 3d2 (Fig. 2, see also [1] and attached pdf file).

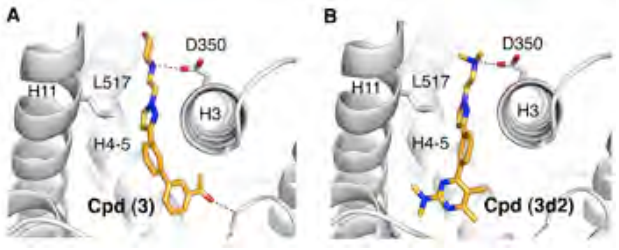

Fig. 1. Predicted mode of binding for Cpd 3 (A) and Cpd 3d2 (B). A cartoon model for LRH-1 polypeptide chain in the vicinity of the ligand-binding pocket is shown in gray, with structural elements forming the pocket indicated. Docked compounds are shown as color-coded stick models.

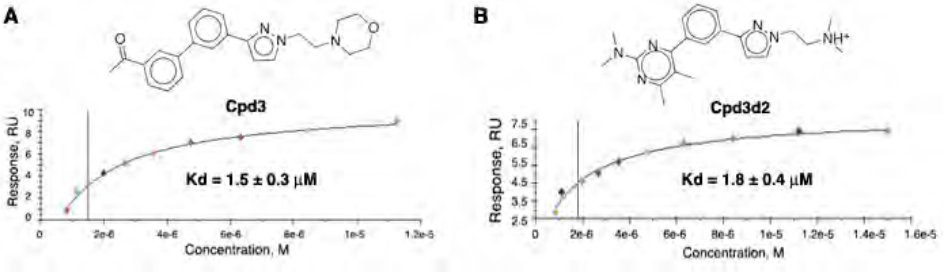

Fig. 2. Evaluation of binding affinity of Cpd 3 (A) and Cpd 3d2 (B). The corresponding chemical structures of compounds are indicated at the top of the panels.

Transcription assay: To verify that these compounds not only bind LRH-1 but also deactivate the receptor upon binding, the transcriptional activity of LRH-1 was assessed in the absence and the presence of Cpd 3 and Cpd

3d2. These experiments showed that treatments with each individual compound lowered the levels of mRNA for G0S2 gene (a transcriptional target of LRH-1) (Fig. 3); the corresponding IC50 values were determined to be 5 ± 1 μM (Fig. 3A) and 6 ± 1 μM (Fig. 3B). To prove that the observed effects by compounds are LRH-1 mediated, the analogous experiments were performed in non-induced HEK293 cells, which do not express the receptor; under these conditions, no significant changes in the levels of G0S2 transcripts were detected in cells treated with either compound compared to the control [1].

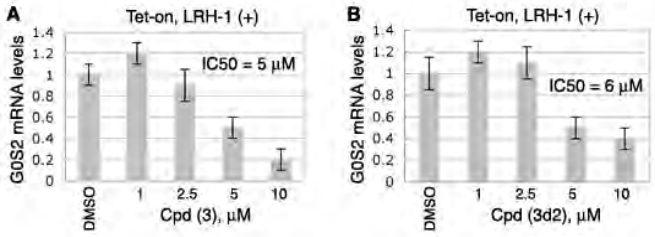

Fig. 3. Effects of Cpd 3 and Cpd 3d2 on transcriptional activity of LRH-1. HEK293 cells expressing LRH-1 (following induction with tetracycline (Tet-on), LRH-1 (+)) were treated with different concentrations of either Cpd 3 (**A**) or Cpd 3d2 (**B**). Following 24 h treatments, levels of mRNA for G0S2 have been evaluated by qPCR relative to control (cells treated with DMSO).

Assessing specificity of Cpd 3 and Cpd 3d2: We examined whether the identified LRH-1 inhibitors exert any effects on transcriptional activities of other nuclear receptors. Using previously published methods, transactivation by three different nuclear receptors – steroidogenic factor 1 (SF-1, a close structural and functional analogue of LRH-1) as well as more distant thyroid hormone receptor beta (TRβ) and androgen receptor (AR) - was assessed in the absence and the presence of Cpd 3 and 3d2. These transcriptional studies presented no evidence of any specific, probe-mediated changes in the transcriptional activities of any of the tested receptors [1]. Based on these data, we conclude that the identified inhibitors bind to the LRH-1 receptor and inhibit its transcriptional activity preferentially.

Aim 2 (Task 2): Testing LRH-1 inhibitors in pancreatic cancer cells.

Because multiple LRH-1 gene targets (including cyclin E1 (Cyc E1), cyclin D1 (Cyc D1) and C-Myc genes) are known to control cell growth and proliferation, we investigated whether treatments of cells with the identified receptor antagonist affects cell proliferation *in vitro* (**Task 2a**). Our previous work [4] demonstrated that selective inhibition of LRH-1 transcription by siRNA arrests growth and proliferation of human pancreatic cancer cells. This receptor-mediated anti-proliferative effect was observed in four different pancreatic ductal adenocarcinoma (PDAC) cell lines, including AsPC-1, which express high levels of LRH-1 [4].

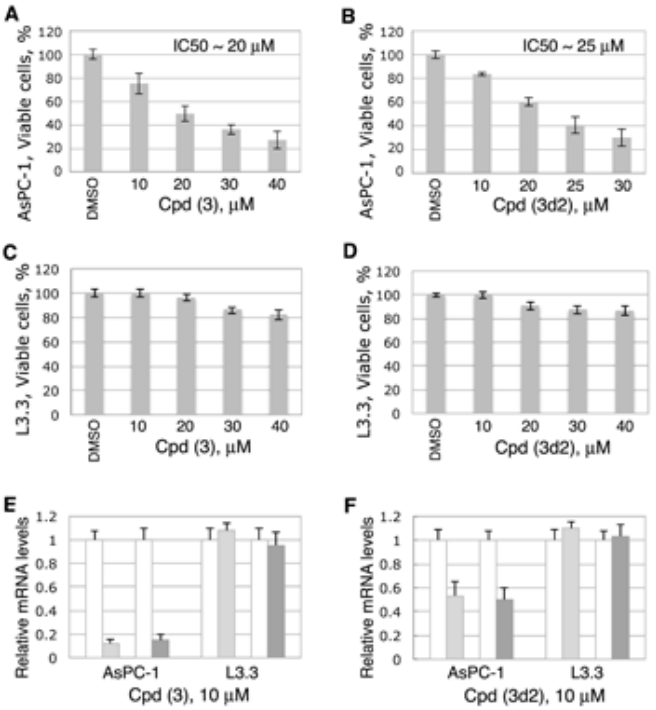

Fig. 4. LRH-1 antagonists inhibit proliferation of pancreatic cancer cells AsPC-1 (LRH-1 positive), but not L3.3 cells (LRH-1 negative). A-D, Cell proliferation rates for both pancreatic cancer cells were measured and compared in the absence and the presence of different concentrations of Cpd 3 (**A, C**) and 3d2 (**B, D**) relative to control (0.1% DMSO). The corresponding IC50 values are indicated. **E, F**, Effects of Cpd 3 (**E**) and 3d2 (**F**) on transcription of the receptor target genes *NR0B2* (encoding SHP) and *CCNE1* (encoding Cyclin E1, Cyc E1) in AsPC-1 and L3.3 cells. Cell samples were analyzed by qPCR for the relative levels of mRNA corresponding to SHP and Cyc E1 following treatments with individual compounds at 10 μM concentration. Controls in white correspond to cells treated with solvent (0.1% DMSO); light and dark gray bars show the levels of mRNA for SHP and Cyc E1 in cells treated with indicated compounds. Data are shown as average of three independent measurements, with experimental errors indicated.

Our current work shows that treatments of AsPC-1 cells with Cpd 3 and 3d2 result in a similar, dose-dependent inhibition of cell proliferation (Fig. 4A, B; concentrations of Cpd 3 and Cpd 3d2 associated with ~50% inhibition of cell proliferation are indicated).

Notably, no significant anti-proliferative effects were observed in pancreatic cancer cells L3.3 (Fig. 4C, D) that do not express LRH-1 receptor at a detectable level [4]. In concert with these data, inhibition of transcription of LRH-1 target genes *NR0B2* and *CCNE1* (encoding SHP and Cyclin E1, in light and dark gray, Fig. 4E, F) was detected in AsPC-1 but not in L3.3 cells following these treatments (**Task 2b**). No general cytotoxicity was encountered for either compound at the concentrations used for these experiments [1]. These results support the idea that the observed anti-proliferative effects of the probes are receptor-mediated and specific.

Our work demonstrates that human pancreatic ductal adenocarcinoma (PDAC) cells expressing LRH-1 are sensitive to treatments with the receptor specific inhibitors, and that growth and proliferation of LRH-1 positive cancer cells could be markedly decreased following such treatments.

The structure-based identification and characterization of the first LRH-1 specific antagonists is described in our recently published research article by Benod *et al.* [1]. This paper reports the use of existing technologies and presents the first specific and potent compounds deriving from computational docking to a non-native protein target structure.

Aim 3 (Task 3): Imaging and optimization of LRH-1 modulators.

During the past year, we worked on optimizing the properties of the identified receptor antagonists and developing new, improved LRH-1 modulators. The goal of this program is to enhance the binding affinities and thus the therapeutic potential of LRH-1 antagonists without compromising their specificity.

Through numerous crystallization trials and complementing biophysical stability evaluations of LRH-1 bound by Cpd3 and Cpd3d2 (see Figs 1, 2) we have learnt that these **antagonistic compounds destabilize the receptor irreversibly upon binding.** Whereas the receptor destabilization contributes to the antagonizing mechanisms by these compounds (Figs. 3, 4), the diminished protein stability compromises its crystallization and the following structural analyses (**Tasks 3a, 3b, 3c, 3d**).

To overcome this limitation, we are employing an alternative approach for developing potent LRH-1 modulators (**Task 3e**): we are designing and testing specific, high affinity LRH-1 agonists first; these compounds stabilize the receptor upon binding, aiding in protein crystallization and the following high-resolution structural analyses. Once the LRH-1 LBD is imaged bound by selected agonist leads, potent receptor antagonists will be designed and developed based on analyses of the binding determinants of the agonistic ligands.

Substantial progress has been made towards this goal. Our new structure of LRH-1 ligand binding domain (LBD) bound by the receptor's hormone - signaling phospholipid PIP3 - explains why preceding efforts failed to find adequate LRH-1 agonists. This structure (as well as our recently published structure of the closest LRH-1 homolog – nuclear receptor SF-1 bound by PIP3 [2]) reveals that the receptor's ligand-binding pocket is comprised of three distinct segments, and that the hormone spans all three segments, stabilizing the active conformation of the LBD (Figs. 5, 6).

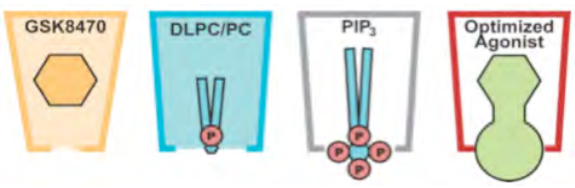

Fig. 5. Effects of bound ligands on LRH-1 structure. Cartoons showing relative locations of the upper (with synthetic ligand, in orange), middle (bound by dietary lipid DLPC, blue) and lower (occupied by the head group of PIP3) segments of the LRH-1 hormone-binding pocket. An optimized receptor modulator spanning all segments of the pocket is shown in green.

This work confirms our earlier hypothesis that bound phospholipids influence the architecture and stability of the LRH-1 hormone-binding pockets, affecting folding of the receptor LBD (Fig. 6). Furthermore, the crystalstructures of NR5A homolog receptors LRH-1 and SF-1 bound to PIP3 [2, 3] revealed the ligand head

group exposed on the receptor surface, organizing a new regulatory scaffolding site (AF-3 in Fig. 6). We consider this new structural information vital for developing optimized LRH-1 ligands, as the structure suggests that **ligands spanning all three segments of the pocket are needed to support optimal LRH-1 function**.

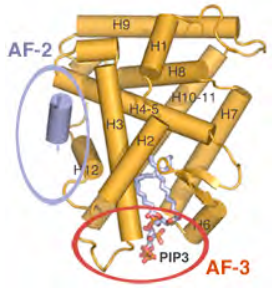

Fig. 6. Structure of PIP3 bound LRH-1. The polypeptide chain of LRH-1 is drawn as a cartoon model; bound PIP3 is shown as a stick model and indicated. Previously identified co-regulator binding site – AF-2 with bound co-regulatory peptide is indicated in blue. The location of the newly identified AF-3 site organized by the exposed PIP3 head group is indicated in red.

Guided by the PIP3-LRH-1 structure, in collaboration with UCSF medicinal chemists (Dr. P. England's lab), we are designing novel LRH-1 ligands using a novel approach - the Fixed Point Buildout method, involving Tethering chemistry (Fig. 7).

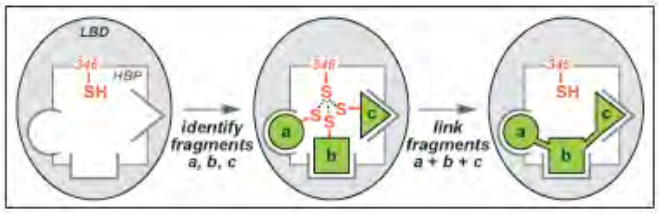

Fig. 7. Tethering scheme. Tethering is a new approach for identifying potent ligands for protein targets. This method relies on the formation of a disulfide bond between individual drug fragments and cysteine residues in the protein. "Hit" fragments are then synthetically elaborated to produce ligands with desired properties.

LRH-1 is an excellent candidate for Tethering, as it has an endogenous tether point - Cys346, which is ideally located inside the receptor pocket. The England lab already screened the Tethering library and identified 20 fragments that: 1) tether exclusively to Cys346, 2) bind with high-affinity to LRH-1, and 3) bind to distinct sub-sites within the pocket. We note that the optimized, full-size ligands do not rely on the covalent attachment to the receptor, as the tethering link may be omitted from the final compound once strong binding affinity is achieved. Consistent with this notion, small scale SAR study based on the identified fragments produced a lead compound (FC 4.171, Fig. 8) that binds to LRH-1 in the absence of the tethering link.

Fig. 8. Evaluation of FC 4.171 binding to LRH-1 by Biacore. Purified apo-LRH-1 LBD was covalently immobilized to the surface of a CM5 chip using a standard amine coupling protocol. Solutions of FC 4.171 at 1 – 20 μM concentrations were injected over immobilized LRH-1 and reference surfaces, and dose-dependent steady-state binding responses recorded and measured relative to the reference. The equilibrium dissociation constant (KD, indicated) was determined using steady state analysis of binding affinities, assuming 1:1 ligand - protein stoichiometry.

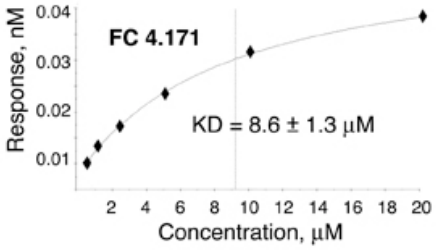

Crystallization trials on LRH-1 bound by FC 4.171 are in progress. Once the structure of LRH-1 LBD bound by FC 4.171 is determined, we will design and test compounds that are expected to perturb specific regulatory sites of LRH-1 upon binding into the receptor ligand-binding pocket (Fig. 9).

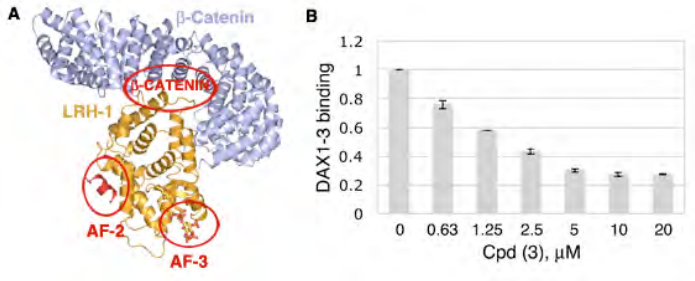

Fig. 9. Targeting regulatory sites of LRH-1. A. Cartoon model of LRH-1 LBD bound by coregulator peptide, hormone PIP3, and β-catenin. Locations of the corresponding regulatory sites, AF-2, AF-3 and β-catenin binding interface, are indicated. **B**. Cpd3 diminishes binding of coregulator peptide to the AF-2 site of LRH-1 in a Biacore based SPR assay. Grey bars indicate binding peptide in presence of different concentrations of Cpd3.

In particular, we aim to disrupt the *interaction of LRH-1 with β-catenin* (indicated in Fig. 9A); in preceding studies, the PI's lab determined the structure of the LRH-1/β-catenin complex and defined the molecular mechanism of this regulatory interaction [5]. We also aim to perturb the *co-activator binding site* (AF-2, Fig. 9A) as well as the *newly identified regulatory site* (AF-3, Fig. 9A) organized by the bound LRH-1 hormone

PIP3 [2, 3]. Perturbation of either of these sites is expected to disable critical interactions of LRH-1 with transcriptional co-regulators, resulting in the receptor deactivation (exemplified by effects of Cpd 3 on binding of co-regulator peptide to the AF-2 site in Fig. 9B). All designed and synthesized compounds will be evaluated in *in vitro* direct binding assays and tested for their ability to block pancreatic cancer cell proliferation, migration and invasion, as described in our published work [1].

4. KEY RESEARCH ACCOMPLISHMENTS:

a) Using innovative experimental strategies, the first specific synthetic inhibitors of LRH-1 - Cpd 3 and Cpd 3d2 - were discovered and characterized by the PI's lab; we demonstrated that these compounds inhibit transactivation by LRH-1, diminishing expression of the receptor's target genes [1].

b) Chemical biology enabled new science: the identified receptor inhibitors were critical for demonstrating therapeutic potential of LRH-1 in pancreatic cancer. Our work showed that treatments of human LRH-1 positive PDAC cells AsPC-1 with Cpd 3 and Cpd 3d2 result in a dose-dependent inhibition of cell proliferation. No significant anti-proliferative effects were observed in pancreatic cancer cells L3.3 that do not express LRH-1, confirming that the observed anti-proliferative effects are receptor-mediated and specific [1].

c) Based on our published results [1], the first commercial synthetic inhibitor of LRH-1 - Cpd3 - was offered in 2014 by Merck to the research community.

d) A major breakthrough in understanding the molecular mechanisms of LRH-1 regulation occurred in 2014: LRH-1 is a newly "adopted orphan" receptor, as its hormone - signaling phospholipid PIP3 has been identified in collaborative work by our group that imaged NR5A receptors bound by PIP3 [2, 3].

e) Analyses of the PIP3-bound NR5A structures clarify the first step in the mechanism that links transactivation by these receptors to nuclear PIP3 signaling [2, 3].

f) Atomic resolution structure of PIP3-LRH-1 defines a complete architecture of the receptor's hormone pocket, confirming that LRH-1 activity can be modulated by small regulatory molecules [3].

g) Guided by the PIP3-LRH-1 structure, in collaboration with UCSF medicinal chemists (Dr. P. England's lab), we are designing novel, potent LRH-1 antagonists using a novel approach - the Fixed Point Buildout method, involving Tethering chemistry.

5. CONCLUSION:

Because of the involvement of LRH-1 in multiple regulatory pathways associated with tumorigenesis, we proposed to evaluate this receptor as a novel target for pancreatic cancer therapy. The appeal of LRH-1 as a drug target includes its defined ligand-binding pocket, which could be targeted by synthetic modulators. At the time of submission of this application, physiological hormones of LRH-1 were not yet known, and no specific small molecule inhibitors were reported for this receptor.

Research resulting from this award identified the first specific synthetic inhibitors of LRH-1. These compounds were critical for demonstrating therapeutic potential of LRH-1 in pancreatic cancer: our work showed that treatments of human PDAC cells with LRH-1 inhibitors result in inhibition of cancer cell proliferation.

In collaboration with UCSF medicinal chemists, we are optimizing the existing receptor antagonists and designing novel, potent LRH-1 modulators for pre-clinical trials *in vivo*. Once successfully tested in animals, the lead compounds could be advanced to clinical trials and lead to development of novel pancreatic cancer drugs, which would advance existing pancreatic cancer therapeutics. The identified LRH-1 inhibitors could also be used as specific molecular tools for in depth analyses of the receptor-mediated mechanisms driving the progression of pancreatic cancer.

6. PUBLICATIONS, ABSTRACTS, AND PRESENTATIONS:

a. Manuscripts and Abstracts submitted for publication during the period covered by this report resulting from this project.

(1) Lay Press:

1. Study Reveals 'Bellhops' in Cell Walls Can Double as Hormones: Discovery at SLAC's Synchrotron Could Lead to New Drug Designs, Treatments. SLAC News Feature Article, October 6, 2014. https://www6.slac.stanford.edu/news/2014-10-06-study-reveals-bellhops-cell-walls-can-double-hormones.aspx

2. This DoD award to the PI will be highlighted in the upcoming FY14 annual report of CDMRP.

(2) Peer-Reviewed Scientific Journals:

1. Benod C, Carlsson J, Uthayaruban R, Hwang P, Irwin JJ, Doak AK, Shoichet BK, Sablin EP, and Fletterick RJ (2013) Structure-Based Discovery of Antagonists of Nuclear Receptor LRH-1. *J Biol Chem.* 288(27): 19830-19844. DOI: 10.1074/jbc.M112.411686. PMID: 23667258

2. Blind RD, Sablin EP, Kuchenbecker KM, Chiu H-J, Deacon AM, Das D, Fletterick RJ, and Ingraham HA (2014) The signaling phospholipid PIP3 creates a new interaction surface on the nuclear receptor SF-1. *Proc. Natl. Acad. Sci. USA,* 111(42): 15054–15059. DOI: 10.1073/pnas.1416740111. PMID: 25288771

3. Sablin EP, Blind, RD, Chiu H-J, Deacon AM, Das D, Ingraham HA, and Fletterick RJ. Crystal structure of the nuclear receptor LRH-1 bound by signaling phospholipid PIP3. *J. Struct. Biol*. 2014, Submitted.

(3) Invited Articles:

Nothing to report

(4) Abstracts:

Fletterick, RJ et al (2014) Orphan Nuclear Receptor LRLH-1, Beta-Catenin and Antagonists in Pancreatic Cancer, Abstract presented at The Endocrine Society's 96th Annual Meeting & Expo, ICE/ENDO 2014, Chicago, Illinois, 21-24 June.

b. Presentations made during the period covered by this report resulting from this project.

Fletterick, Robert. "Orphan Nuclear Receptor LRLH-1, Beta-Catenin and Antagonists in Pancreatic Cancer" The Endocrine Society's 96th Annual Meeting & Expo, ICE/ENDO, Chicago, IN. 24 June 2014. Invited speaker.

7. INVENTIONS, PATENTS AND LICENSES:

Nothing to report.

8. REPORTABLE OUTCOMES:

The two characterized LRH-1 antagonists - Cpd3 and Cpd3d2 - have been shipped to the National Cancer Institute (NCI) Chemotherapeutic Agents Repository. Under the NCI Developmental Therapeutic Program, both compounds have been selected for anticancer screening in 60 cancer cell lines representing

different types of malignancies, including leukemia, non-small cell lung cancer, colon cancer, CNS cancer, melanoma, ovarian, breast and prostate cancers as well as renal cancer. Although pancreatic cancer cell lines were not part of the tested series, both compounds demonstrated anti-cancer cell proliferative effects in several cell lines known to express the LRH-1 receptor. The acquired data and chemicals are available for the research community.

Based on our published results [1], the first commercial synthetic inhibitor of LRH-1 - Cpd3 - was offered in 2014 by Merck to the research community.

9. OTHER ACHIEVEMENTS:

Cindy Benod, a key scientist on this grant and the first author of the manuscript describing the first specific antagonists of LRH-1 [1], has finished her postdoctoral training in the PI's lab and now holds a Senior Scientist position at the Department of Genomic Medicine, Houston Methodist Research Institute (HMRI), Houston, Texas.

Based on results generated from work supported by this award, the PI is applying for the DOD Breast Cancer Research Program Breakthrough Award as well as an NIH R01 grant in response to the Funding Opportunity Announcement (FOA) "Early-Stage Pharmacological Validation of Novel Targets and Accompanying Pre-Therapeutic Leads for Diseases of Interest to the NIDDK".

10. REFERENCES:

4. Benod C, Vinogradova MV, Jouravel N, Kim GE, Fletterick RJ, and Sablin EP (2011) Nuclear receptor liver receptor homologue 1 (LRH-1) regulates pancreatic cancer cell growth and proliferation. *Proc Natl Acad Sci USA* 108 (41):16927-16931. DOI: 10.1073/pnas.1112047108; PMID: 21949357.
5. Yumoto F, Nguyen P, Sablin EP, Baxter JD, Webb P and Fletterick RJ (2012) Structural basis of coactivation of liver receptor homolog-1 by β-catenin. *Proc Natl Acad Sci USA 109*: 143-148. DOI: 10.1073/pnas.1117036108. PMID: 22187462.

11. APPENDICES:

Attached are PDF files of research articles and scientific abstracts published during the period covered by this report.

Cell Biology:

Structure-based Discovery of Antagonists of Nuclear Receptor LRH-1

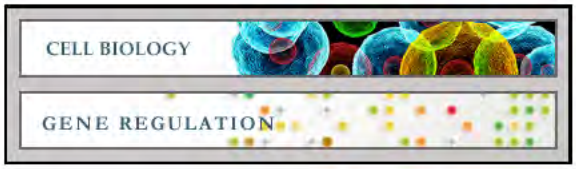

Cindy Benod, Jens Carlsson, Rubatharshini Uthayaruban, Peter Hwang, John J. Irwin, Allison K. Doak, Brian K. Shoichet, Elena P. Sablin and Robert J. Fletterick

J. Biol. Chem. 2013, 288:19830-19844.
doi: 10.1074/jbc.M112.411686 originally published online May 10, 2013

THE JOURNAL OF BIOLOGICAL CHEMISTRY VOL. 288, NO. 27, pp. 19830–19844, July 5, 2013

Structure-based Discovery of Antagonists of Nuclear Receptor LRH-1*

Received for publication, January 28, 2013, and in revised form, May 3, 2013 Published, JBC Papers in Press, May 10, 2013, DOI 10.1074/jbc.M112.411686

Cindy Benod[‡1,2], **Jens Carlsson**[§1,3], **Rubatharshini Uthayaruban**[‡], **Peter Hwang**[‡], **John J. Irwin**[§], **Allison K. Doak**[§], **Brian K. Shoichet**[§], **Elena P. Sablin**[‡], **and Robert J. Fletterick**[‡4]

From the Departments of [‡]*Biochemistry and Biophysics and* [§]*Pharmaceutical Chemistry, University of California at San Francisco, San Francisco, California 94158*

Background: Liver receptor homolog 1 (LRH-1, NR5A2) regulates functions of liver, intestines, and pancreas; its aberrant activity is associated with tumorigenesis.
Results: Our work identifies the first antagonists of LRH-1.
Conclusion: The identified ligands inhibit LRH-1 transcriptional activity, diminishing expression of the receptor's target genes.
Significance: LRH-1 inhibitors could be used for analyses of the receptor's biological mechanisms and for development of cancer therapeutics.

Liver receptor homolog 1 (nuclear receptor LRH-1, NR5A2) is an essential regulator of gene transcription, critical for maintenance of cell pluripotency in early development and imperative for the proper functions of the liver, pancreas, and intestines during the adult life. Although physiological hormones of LRH-1 have not yet been identified, crystallographic and biochemical studies demonstrated that LRH-1 could bind regulatory ligands and suggested phosphatidylinositols as potential hormone candidates for this receptor. No synthetic antagonists of LRH-1 are known to date. Here, we identify the first small molecule antagonists of LRH-1 activity. Our search for LRH-1 modulators was empowered by screening of 5.2 million commercially available compounds via molecular docking followed by verification of the top-ranked molecules using *in vitro* direct binding and transcriptional assays. Experimental evaluation of the predicted ligands identified two compounds that inhibit the transcriptional activity of LRH-1 and diminish the expression of the receptor's target genes. Among the affected transcriptional targets are co-repressor SHP (small heterodimer partner) as well as cyclin E1 (*CCNE1*) and *G0S2* genes that are known to regulate cell growth and proliferation. Treatments of human pancreatic (AsPC-1), colon (HT29), and breast adenocarcinoma cells T47D and MDA-MB-468 with the LRH-1 antagonists resulted in the receptor-mediated inhibition of cancer cell proliferation. Our data suggest that specific antagonists of LRH-1 could be used as specific molecular probes for elucidating the roles of the receptor in different types of malignancies.

Liver receptor homolog 1, commonly known as LRH-1[5] or NR5A2, is a member of the nuclear receptor family of regulatory transcription factors (1). In adults, this protein is expressed primarily in liver, intestine, and pancreas, where it controls expression of proteins maintaining cholesterol and bile acid homeostasis as well as production of pancreatic enzymes (1, 2). LRH-1 is also expressed in the ovary and breast adipose tissue where it controls biosynthesis of steroids (3, 4). LRH-1 is vital in early development as it maintains a pool of undifferentiated embryonic stem (ES) cells by controlling expression of two master transcription factors, POU5F1 (known as OCT3/4) and NANOG (5–7). Recent studies demonstrated that LRH-1 can substitute for POU5F1 in derivation of induced pluripotent stem cells (7).

Because of its decisive role in cell differentiation, LRH-1 is linked to multiple developmental pathways, including Hedgehog (8) and Wnt/β-catenin (6, 9, 10) signaling. In particular, LRH-1 enhances transcription of multiple genes controlled by the regulatory Wnt/β-catenin cascade. The established transcriptional targets of LRH-1 paired with β-catenin include *CCND1* and *CCNE1* genes as well as *MYC* genes known for controlling cell differentiation, growth, and proliferation (6, 7, 9). Because these developmental pathways and associated genes are re-activated during tumorigenesis (11–16), an aberrant activity of LRH-1 is linked to different types of malignancies, including breast and endometrial cancers as well as intestinal tumors and cancer of the pancreas (17–24). The LRH-1 recep-

* This work was supported, in whole or in part, by National Institutes of Health Grants GM59957 (to B. K. S.) and R01 DK078075 and R21 CA140751 (to R. J. F.). This work was also supported by Department of Defense Grant W81XWH-12-1-0396 (to R. J. F.), by a fellowship from the California Breast Cancer Research Program (to C. B.), and a fellowship from the Knut and Alice Wallenberg Foundation (to J. C.).
[1] Both authors contributed equally to this work.
[2] Present address: Dept. of Biochemistry and Biophysics, Center for Nuclear Receptors and Cell Signaling, The Methodist Hospital Research Institute, 6670 Bertner St., Houston, TX 77030.
[3] Present address: Center for Biomembrane Research, Stockholm University, 106 91 Stockholm, Sweden.
[4] To whom correspondence should be addressed: Dept. of Biochemistry and Biophysics, University of California San Francisco, 600 16th St., GH S412E, San Francisco, CA 94158-2517. Tel.: 415-476-5080; Fax: 415-476-1902; E-mail: Robert.Fletterick@ucsf.edu.

[5] The abbreviations used are: LRH-1, liver receptor homolog 1; LBD, ligand-binding domain; ERα, estrogen receptor α; PDB, Protein Data Bank; Tet, tetracycline; TRβ, thyroid hormone receptor β; DSF, differential scanning fluorimetry; E2, estradiol; SPR, surface plasmon resonance; AR, androgen receptor; Cpd, compound; CCF, Cell Culture Facility; Pen/Strep, penicillin/streptomycin; h, human; DLS, dynamic light scattering; LBP, ligand-binding pocket; qPCR, quantitative PCR; AmpC, AmpC β-lactamase; SHP, small heterodimer partner.

tor is also implicated in development of various metabolic disorders related to insufficient liver and pancreas functions (25–27). Because of the critical roles of this receptor in human physiology and pathophysiology, identification of specific regulatory ligands, modulators of LRH-1 transcriptional activity, is extremely important.

LRH-1 is classed as an orphan nuclear receptor because its activating hormones (physiological agonists) have not yet been identified. Crystallographic and biochemical studies presented compelling evidence that LRH-1 could bind regulatory ligands (27–32) and suggested phosphatidylinositols as potential hormone candidates for this receptor (29). Studies in mice showed that dilauroyl phosphatidylcholine stimulates LRH-1 activity, increasing bile acid levels, lowering hepatic lipids, and improving glucose homeostasis (27, 28). LRH-1 is also regulated via post-translational modifications, including phosphorylation and sumoylation (33, 34). Specifically, phosphorylation of the regulatory hinge region (connecting the ligand- and DNA-binding domains of LRH-1) by MAPK/ERK stimulates the receptor's transcriptional activity (33), whereas sumoylation of this region results in receptor inhibition (34). Known transcriptional regulators of LRH-1 include co-activators steroid receptor co-activators (SRCs), CREB-binding protein (CBP), and peroxisome proliferator-activated receptor γ co-activator-1α (*PGC-1a*) as well as co-repressors silencing mediator of retinoid and thyroid hormone receptors (SMRT), SHP, prospero-related homeobox 1 (*PROX1*), and dosage-sensitive sex reversal, adrenal hypoplasia critical region, on chromosome X, gene 1 (*DAX1*) (1, 35, 36). No synthetic antagonists of LRH-1 are available to date.

Here, we describe the first synthetic antagonists of LRH-1. Candidate modulators have been identified using screening by molecular docking against a model of the LRH-1 ligand-binding domain (LBD) in an antagonized conformation. This computational screening was followed by direct binding, transcription, and cell proliferation studies *in vitro*. The results described and discussed in this work suggest that specific antagonists of LRH-1 could be developed for studies of the receptor's biological mechanisms as well as therapeutic treatments.

EXPERIMENTAL PROCEDURES

Molecular Docking Calculations—DOCK3.6 (37–40) was used to screen a library of commercially available compounds against a model of LRH-1 LBD in a transcriptionally inactive conformation. The flexible ligand sampling algorithm in DOCK3.6 superimposes atoms of the docked molecule onto spheres matching a defined binding site; these spheres represent favorable positions for individual ligand atoms (39, 40). Fifty matching spheres mimicking the inside of the receptor ligand-binding pocket (LBP) were used for the molecular docking calculations. The positions of the spheres were dictated by the conformation of the phospholipid bound in the LRH-1 LBP (PDB code 1YUC (30)) and were re-adjusted manually to increase sampling at the opening in the receptor's molecular surface created by deletion of its helix H12 (see "Results"). The accuracy of ligand sampling is determined by the bin size, bin size overlap, and distance tolerance; these three parameters were set to 0.2, 0.1, and 1.4 Å, respectively, for both the binding site matching spheres and the docked molecules. For ligand conformations passing an initial steric filter, a physics-based scoring function was used to evaluate the fit to the binding site. For the best scoring ligands and conformations, 100 steps of rigid-body minimization were carried out prior to assignment of the final score. The score for each conformation was calculated as the sum of the receptor-ligand electrostatic and van der Waals interaction energies, corrected for ligand desolvation; the latter three terms were deduced from pre-calculated grids, as described previously (37). Partial charges from the united atom AMBER force field (41) were used for all receptor atoms (except for Val-406, for which the polarity of the backbone atoms was increased by adding +0.4 and −0.4 electrons to the partial charges of hydrogen and oxygen atoms, respectively, of the peptide bond).

A library of 5.2 million commercially available molecules from the ZINC database (42) was screened against the LRH-1 LBD model. The screen included two sets of compounds; the first set was composed of compounds with molecular weight (M_r) less than 400 (with predicted logP value less than 4, and less than 10 rotatable bonds); the second set included molecules with M_r between 350 and 400 and a predicted logP value between 4 and 5. Prior to docking, subsets of up to 1000 conformations for each molecule were prepared using the program OMEGA (OpenEye Scientific Software). Partial atomic charges and transfer free energies for each ligand atom have been calculated using AMSOL (43) and van der Waals parameters determined using an all-atom potential from AMBER (44).

Protein Expression and Purification—Recombinant nuclear receptors LRH-1 and SF-1 were expressed and purified using similar methods. In brief, cDNA encoding human LRH-1 LBD (amino acids 294–541) was cloned into pRSF-2 Ek/LIC (Novagen) vector containing the N-terminal His_6 tag followed by tobacco etch virus protease cleavage site. The recombinant protein was expressed in BL21(DE3) cells using standard methods (induction with 0.1 mM isopropyl 1-thio-β-D-galactopyranoside followed by overnight cell culturing at 16 °C) and purified using Ni^{2+}-nitrilotriacetic acid affinity column (Qiagen) followed by size exclusion chromatography (HiLoad 16/60 Superdex 200, GE Healthcare) in buffer containing 20 mM Tris, pH 8.0, 150 mM NaCl, 5 mM DTT, 10% glycerol and 2 mM CHAPS.

cDNA encoding human SF1 LBD (hSF-1, amino acids 218–461) was cloned into pET-46 Ek/LIC (Novagen) vector containing His_6 tag followed by a tobacco etch virus protease cleavage site. The recombinant protein was expressed and purified as described above.

Mutagenesis—cDNA encoding wild type hLRH-1 LBD (amino acids 294–541) in pRSF-2 vector (Novagen) and the QuikChange site-directed mutagenesis kit (Stratagene) were used for generating mutants A349F (forward and reverse primers 5′-GGG CTT ATG TGC AAA ATG TTC GAT CAA-3′ and 5′-GGA GAA GAG AGT TTG ATC GAA CAT TTT-3′) and A349W (forward and reverse primers 5′-GGG CTT ATG TGC AAA ATG TGG GAT CAA-3′ and 5′-GGA GAA GAG AGT TTG ATC CCA CAT TTT-3′). The introduced mutations were verified by sequencing, and the mutant proteins were expressed and purified as described above for wild type LRH-1.

Differential Scanning Fluorimetry (DSF)—Protein stability in the presence and the absence of tested compounds was assessed using the DSF method, MxPro3005P qRT-PCR detection system (Stratagene) in a 96-well format. Sypro-Orange dye (Invitrogen) was used to monitor the fluorescence, with carboxyfluorescein (FAM) filter for fluorescence excitation (492 nm) and carboxy-X-rhodamine (ROX) filter for fluorescence emission (610 nm). The DSF spectra for purified wild type and mutant variants of hLRH-1 LBD (10 μM) were recorded using screening buffer (TBS) with added Sypro-Orange dye (1:2000 dilution), in the presence of individual compounds (100 μM) or 1% DMSO (control). Tested sample mixtures (final volume 50 μl) were heated gradually, from 25 to 96 °C, at the rate of 2 °C/min, and the corresponding fluorescence was recorded following every 1 °C increase. The melting temperature (T_m) for each sample was deduced by the KaleidaGraph program (Synergy) from the first derivative of the corresponding denaturation curve generated by the MxPro QPCR software (Stratagene).

Surface Plasmon Resonance—SPR was used for quantification of direct binding of compounds 3 and 3d2 to hLRH-1 LBD. Measurements were performed on a Biacore T100 instrument, with a running buffer of 20 mM Tris-HCl, pH 8.0, 150 mM NaCl, 5 mM DTT, 5% DMSO, and 0.05% Tween 20, at 10 °C. The purified LRH-1 protein (either wild type or mutant LBD) was covalently immobilized to the surface of a CM5 biosensor chip to a surface density of about 3000 resonance units, using standard amine coupling chemistry. The individual compounds at 0.8–15 μM concentrations were injected over immobilized LRH-1 and reference surfaces, and binding response sensorgrams were solvent-corrected against running buffer with DMSO concentrations ranging from 4.9 to 5.1%. The corresponding equilibrium dissociation constants (K_d) were determined using steady-state analysis of the compounds' binding affinities, assuming 1:1 ligand-protein stoichiometry. Prior to evaluations of binding affinities of compounds, the functionality of immobilized LRH-1 protein was confirmed by demonstrating its high affinity interactions with a peptide DAX1–3 corresponding to amino acids ^{140}PRQGSILYSLLTSSK^{154} of the receptor's transcriptional co-regulator *DAX-1*.

Evaluation of the effects of compounds 3 and 3d2 on binding of DAX1–3 peptide to LRH-1 was performed using a Biacore T200 instrument at 25 °C, with the running buffer described above. The purified LRH-1 protein was covalently immobilized to the surface of a CM5 biosensor chip to a surface density of about 1000 resonance units, using standard amine coupling chemistry. Solutions of DAX1–3 peptide at 100 nM concentration in the presence of either 5% DMSO (solvent control) or individual compounds at different concentrations (0.063–40 μM) were injected over immobilized LRH-1 and reference surfaces; binding response sensorgrams were recorded and quantified using the Biacore T200 software.

Fluorescence Anisotropy Assay—Fluorescence polarization ligand binding assay was used to determine whether compounds 3 and 3d2 bind human estrogen hormone receptor α. The assay was performed using the Polarscreen™ ERα competitor assay, green kit (Invitrogen), according to the manufacturer's protocol. Serial dilutions of estradiol (E2, positive control) and individual compounds in DMSO were prepared and transferred to the wells of a black OptiPlate™ 384F plate (PerkinElmer Life Sciences) containing E2 Screening Buffer. Following addition of Fluormone™ E2-ERα complex to each well (4.5 nM E2, 15 nM ERα), the assay plate was incubated for 2 h in the dark, and polarization values were measured using a EnVision® multilabel reader (PerkinElmer Life Sciences). All measurements were done in triplicate and the data fit using Prism software (GraphPad Software).

Transactivation Assays—Two (Tet)-inducible HEK293 cell lines expressing full-length hLRH-1 or hSF-1 receptors, respectively (32), were plated into 12-well tissue culture plates in batches of 10^5 cells. After 24 h, tetracycline (Sigma) at a final concentration of 10 nM was added to each well to induce the expression of hLRH-1 or hSF-1. Three hours after the induction, cells were treated with either individual compounds (at concentrations 1–10 μM) or DMSO (0.1%, control). Following 24 h of incubation with compounds, cells were lysed, total RNA was isolated and the corresponding cDNA synthesized, and mRNA levels for *G0S2* (in cells expressing hLRH-1) or *NR0B2* (encoding SHP, in cells expressing hSF-1) genes in each sample were assessed by qPCR (see under "RNA Purification, cDNA Synthesis and qPCR Analysis").

For a transactivation assay with estrogen hormone receptor α (45), transient co-transfections of HeLa cells with vectors encoding either Gal4 DNA-binding domain (DBD) or Gal4 DBD-hERα LBD fusion (gift from Dr. S. Ayers, The Methodist Hospital Research Institute, Houston, TX), both at 10 ng/well, constructs for *Gal4-E1B* promoter linked to a luciferase reporter gene (200 ng/well) and actin β-galactosidase (10 ng/well, internal control) were performed in batches of 10^5 cells seeded into 12-well tissue culture plates. The transfections were done using FuGENE HD transfection reagent (Promega), and the transfection efficiencies were assessed by measuring the corresponding activity of β-galactosidase. At 3 h after the transfections, cells were treated with either DMSO (0.1%, control) or individual compounds at different concentrations, in the presence of E2 (10 nM), in the medium containing no fetal bovine serum. Following 24 h of incubation, luciferase activities in each well were assessed using the luciferase assay system (Promega) relative to the control. Cells transfected with Gal4 DBD vector served as a control for ERα-independent effects.

For a transcription assay with androgen hormone receptor (46), transient co-transfections of HeLa cells with vectors encoding either Gal4 DBD or Gal4 DBD-hAR LBD fusion (both at 10 ng/well), constructs for GK1 reporter (200 ng/well) and actin β-galactosidase (10 ng/well, internal control) were performed in batches of 10^5 cells seeded into 12-well tissue culture plates. The transfections were done using TransFectin lipid reagent (Bio-Rad), and the transfection efficiencies were assessed by measuring the corresponding activity of β-galactosidase. Three hours after the transfections, cells were treated with either DMSO (0.1%, control) or compounds 3 or 3d2 at different concentrations, in the absence or the presence of dihydrotestosterone (1 μM). Following 24 h of incubation, luciferase activities in each well were assessed using the luciferase assay system (Promega) relative to the control. Cells transfected with Gal4 DBD vector served as a control for AR-independent effects.

For a transcription assay with thyroid hormone receptor β (46), transient co-transfections of HeLa cells with vectors encoding either Gal4 DBD or Gal4 DBD-hTRβ LBD fusion (both at 10 ng/well), constructs for GK1 reporter (200 ng/well), and actin β-galactosidase (10 ng/well, internal control) were performed in batches of 10^5 cells seeded into 12-well tissue culture plates. The transfections were done using TransFectin lipid reagent (Bio-Rad), and the transfection efficiencies were assessed by measuring the corresponding activity of β-galactosidase. After 3 h, cells were treated with either DMSO (0.1%, control) or compounds 3 or 3d2 at different concentrations, in the absence or the presence of T3 (1 μM). Following 24 h of incubation, luciferase activities in each well were measured using the luciferase assay system (Promega) relative to the control. Cells transfected with Gal4 DBD vector served as a control for TRβ-independent effects.

RNA Purification, cDNA Synthesis, and qPCR Analysis—Total RNA from different cell samples was isolated using TRIzol reagent (Invitrogen) according to the manufacturer's protocol. cDNA was synthesized from 500 ng of total RNA at 42 °C for 60 min in the presence of random primers (Invitrogen) using the SuperScript-II reverse transcriptase (Invitrogen). Quantitative PCR amplification of mRNA for *G0S2*, *NR0B2*, *CCNE1*, and *RPS9* (ribosomal protein S9 gene, internal control) was performed in triplicates using the Mx3005P real time PCR system (Stratagene) and the SYBR Green I dye for detection (Stratagene). Specific oligonucleotides used for these experiments were as follows: for *CCNE1* (PPH00131A-200, SABiosciences), *G0S2* (5′-CAGAGAAACCGCTGACATCTAGAA-3′ and 5′-CAGCAAAACTCAATCCCAAACTC-3′, IDT), *NR0B2* (PPH05889A-200, SABiosciences), and *RPS9* (5′-AAGGCCGCCCGGGAACTGCTGAC-3′ and 5′-ACCACCTGCTTGCGGACCCTGATA-3′, IDT). To control for external contamination, no template control and no reverse transcription control were included in each run. The amplification curves were analyzed with the Mx3005P software using the comparative cycle threshold (*Ct*) method. Relative quantification of the target mRNAs was evaluated after normalization of *Ct* values with respect to the *RPS9* levels.

Promiscuous Inhibition Test—To exclude fortuitous inhibition by tested compounds due to their possible colloidal aggregation, dynamic light scattering method (DLS) was employed to assess particle formation in solutions of tested compounds. In addition, a standard enzymatic assay was performed to detect any unspecific inhibition of AmpC β-lactamase by these ligands. For DLS experiments, concentrated DMSO stocks of compounds were diluted with filtered buffer used for quantitative Biacore-based direct binding assay (20 mM Tris-HCl, pH 8.0, 150 mM NaCl, 5 mM DTT, 5% DMSO, 0.05% Tween 20). Measurements were made using a DynaPro MS/X instrument (Wyatt Technology), with a 55-milliwatt laser (100% power) at 826.6 nm and a 90° detector angle. Inhibition of AmpC β-lactamase was assessed in 50 mM potassium phosphate, pH 7.0. Individual compounds (100 μM solutions in 1% DMSO) were incubated with 1 nM β-lactamase for 5 min, and reactions were initiated by adding the substrate CENTA (Chromothin, Tydock Pharma). To assess enzyme inhibition, the absorbance at 405 nm was recorded for 5 min using a spectrophotometer (Agilent). The assay was performed in 1-ml cuvette duplicates, with controls measuring enzyme activity in the presence of solvent (1% DMSO).

Cell Line Maintenance—Human pancreatic cancer cell lines AsPC-1 and L3.3 were kindly provided by Dr. M. McMahon (Helen Diller Family Comprehensive Cancer Center, University of California at San Francisco); cells were cultured at 37 °C in a humidified atmosphere containing 5% CO_2, in DMEM (University of California at San Francisco Cell Culture Facility (CCF)) supplemented with 10% fetal bovine serum (FBS, Hyclone), 1× L-glutamine, and 1× Pen/Strep antibiotics (from 100× stocks, CCF). Human breast cancer cells T47D were purchased from the CCF and maintained in RPMI 1640 media (CCF) with 10% FBS (Hyclone), 1× Pen/Strep antibiotics, and 0.2 IU/ml insulin (CCF). Human breast cancer cells MDA-MB-458 were purchased from the CCF and maintained in Leibovitz's L-15 medium without $NaHCO_3$ (CCF) supplemented with 10% FBS (Hyclone), 1× Pen/Strep antibiotics, 1× L-glutamine (CCF), and 3.7 g/liter $NaHCO_3$ (CCF). Human colon adenocarcinoma cells HT-29 were purchased from the CCF and maintained in McCoy's 5A medium (CCF) supplemented with 10% FBS (Hyclone) and 1× Pen/Strep antibiotics (CCF). Tet-inducible HEK293 cell lines expressing either hLRH-1 or hSF-1 receptors were kindly provided by Dr. H. Ingraham (Dept. of Cellular and Molecular Pharmacology, University of California at San Francisco) and maintained in DMEM (Invitrogen) supplemented with 10% Tet-negative FBS (Hyclone), 1× Pen/Strep antibiotics (CCF), 5 μg/ml blasticidin (Invitrogen), and 50 μg/ml hygromycin (Invitrogen); for cells expressing hSF-1, extra 1× sodium pyruvate (CCF) and 1× nonessential amino acids solution (CCF) were added to the medium. HeLa cells were kindly provided by Phuong Nguyen (Fletterick Laboratory, Department of Biochemistry and Biophysics, University of California at San Francisco) and maintained in DMEM H-21 (CCF) supplemented with 10% charcoal, dextran-stripped FBS (Hyclone), and 1× Pen/Strep antibiotics (CCF). All cells were passaged when they reached 80% confluence and harvested using a solution containing 0.05% trypsin and EDTA.

Cell Proliferation Assays and Cytotoxicity Measurements—For cell proliferation assays, cells were plated in 96-well microtiter plate triplicates, at a density of 10^4 cells/ml. Three hours after the plating, cells were treated with individual compounds at different concentrations or with DMSO (control); 24, 48, 72 and 96 h following the treatments, cell proliferation in each well was quantified using the CellTiter-Glo reagent (Promega). Cell proliferation rates for treated cells were compared with those of the control cells. For cytotoxicity measurements, cells were plated in 96-well microtiter plate triplicates, at a density of 10^4 cells/ml; cells were then treated with different concentrations of tested compounds or DMSO (control), and 24 h following the treatments, cytotoxicity was assessed using the CytoTox-Glo cytotoxicity assay reagent (Promega).

RESULTS

Modeling of the hLRH-1 LBD in a Transcriptionally Inactive Conformation—All available crystal structures of the LRH-1 LBD represent the receptor in its active state (with the C-terminal helix H12 tightly packed against helices H3, H4–H5, and

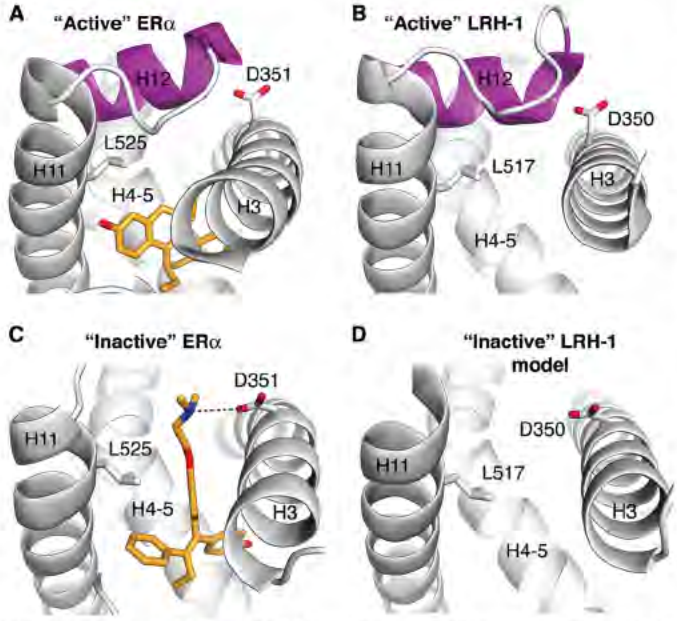

FIGURE 1. **Design of a model for LRH-1 ligand-binding pocket in an antagonized state.** *A,* architecture of the pocket of ERα with bound agonist. A schematic model for ERα polypeptide chain (ERα LBD bound by *R,R*-5,11-*cis*-diethyl-5,6,11,12-tetrahydrochrysene-2,8-diol, PDB code 1L2I) is shown in *gray*; structural elements forming the pocket (H3, H4–H5, H11, and H12) are indicated; helix H12 docked in the "active" conformation is highlighted in *magenta*. Bound agonist is shown as a *stick model*. *B,* architecture of the hormone-binding pocket of LRH-1 in transcriptionally active state. A schematic model for LRH-1 polypeptide chain (PDB code 1YUC) is shown in *gray*, with structural elements forming the pocket indicated. Helix H12 docked in the active conformation is highlighted in *magenta*. *C,* architecture of the hormone-binding pocket of ERα with antagonist 4-hydroxytamoxifen bound in the pocket. Structural elements forming the ligand-binding pocket of ERα (PDB code 3ERT) are indicated. Bound antagonist is shown as a *stick model*. An alternative conformation for side chain of Asp-351 facilitating binding interactions of ERα with 4-hydroxytamoxifen is indicated. *D,* model for the hormone-binding pocket of LRH-1 in transcriptionally inactive state. Undocked helix H12 is omitted from the model. Alternative conformations for side chains of Leu-517 and Asp-350 predicted to facilitate binding interactions of LRH-1 with potential ligands-antagonists are indicated.

H11, poised for interactions with transcriptional co-activators) (28–32). Furthermore, all known LRH-1 ligands, identified either in structural or functional studies, are receptor agonists stabilizing its active conformation (27–32). Thus, to enable identification of LRH-1 antagonists via structure-based virtual screening, we generated a model of a transcriptionally inactive state of the receptor LBD. Based on the structural similarity between LRH-1 and estrogen receptor α (ERα) LBDs (Fig. 1, *A* and *B*), we hypothesized that these receptors could be antagonized in a similar manner. Numerous antagonists have been developed against ERα, and independent atomic resolution structures of ERα have been determined with individual antagonists bound in the receptor's ligand-binding pocket (47–49) (illustrated by ERα bound by receptor antagonist 4-hydroxytamoxifen (PDB code 3ERT (47)) in Fig. 1*C*). The ERα antagonists typically have a hydrophobic core, which is connected to a bulky and often polar "side chain." Whereas the hydrophobic core binds in the ligand-binding cavity of the receptor, the side chain, which cannot be contained within the pocket, protrudes out of the cavity. As a consequence, helix H12 is sterically hindered from aligning in the proper agonist conformation, precluding binding of co-activators to ERα. By analogy, the inactive state for LRH-1 LBD was modeled by undocking helix H12 (amino acids 524–538) from a structure of the receptor LBD in transcriptionally active conformation (PDB code 1YUC (30)) (Fig. 1*D*). Because different orientations for H12 have been observed for estrogen receptor bound by different antagonists (47–50) (including those that completely abolished the association between H12 and the rest of the LBD (50)), helix H12 of LRH-1 was omitted from the model. In addition, side chains of Leu-517 and Asp-350 were re-positioned in the LRH-1 LBD to match their counterparts in the structure of antagonist-bound ERα (Fig. 1, *C* and *D*). These structural re-arrangements are thought to facilitate binding of a potential antagonist to the LRH-1 LBD, in particular, by enabling favorable electrostatic interactions between the antagonist's polar moiety and the re-oriented carboxylate group of Asp-350. In the active conformation of LRH-1, this conserved residue (Asp-351 in ERα, Fig. 1, *A* and *B*) registers and stabilizes the proper orientation of helix H12 by making hydrogen bonds with the main chain of H12 at its base.

Virtual Screening and Compound Selection—DOCK3.6 (37–40) was used to screen 5.2 million commercial compounds from the ZINC database (42) against our model of the inactive state of hLRH-1 LBD. For each screened molecule, ~2800 orientations have been sampled, and for each of these, ~18,000 conformations were scored. The molecules were ranked based on the sum of their van der Waals and electrostatic interaction energies corrected for ligand desolvation (see under "Experimental Procedures"). The top ranked 10,000 compounds (0.2% of the compound library) were then post-processed to identify molecules that could not be accommodated by the active conformation of the receptor (PDB code 1YUC (30)) and that had the potential to displace helix H12 from its active orientation. This was accomplished by selecting compounds capable of forming a favorable electrostatic interaction with the LRH-1 residue Asp-350 (shown for two docked candidate compounds in Fig. 2); the analogous electrostatic bridge is a characteristic feature of many ERα-antagonist complexes (indicated in Fig. 1*C* for ERα bound by 4-hydroxytamoxifen). Following visual inspection of the resulting top-ranked 1000 compounds (0.02% of the initial library content), eight were selected for experimental evaluations (compounds 1–8, Table 1). The criteria for this manual selection process were as follows: 1) clear structural complementarity between a considered compound and the receptor ligand-binding pocket; 2) a strong predicted interaction of a candidate compound with the LRH-1 Asp-350 (to favor antagonism), and 3) immediate availability of compounds for experimental evaluations.

Three Out of Eight Predicted Antagonists Bind Directly to hLRH-1 LBD—Using the DSF method, we analyzed binding of each of the eight selected compounds to the purified recombinant hLRH-1 LBD. Preceding these experiments, the proper folding and functionality of the purified LRH-1 protein were assessed by the DSF and fluorescence anisotropy methods. Using the DSF-based quality control, we analyzed the protein's melting curve and determined its transition temperature (T_m). This analysis showed that in the presence of 1% DMSO (solvent control), hLRH-1 LBD has a stable base line, a transition at 53.4 ± 0.1 °C (reference T_m), and a sloped denatured base line. Following the DSF-based protein folding control, the function-

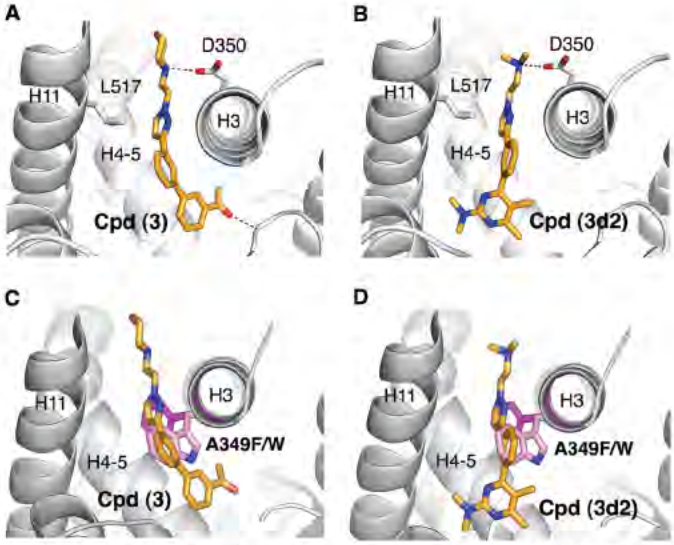

FIGURE 2. **Predicted mode of binding for the identified LRH-1 antagonists.** *A* and *B*, schematic model for LRH-1 polypeptide chain in the vicinity of the hormone-binding pocket is shown in *gray*, with structural elements forming the pocket indicated. Docked receptor antagonists (compound 3 in *A* and compound 3d2 in *B*) are shown as color-coded *stick models*. Side chains of Leu-517 and Asp-350 predicted to facilitate binding interactions of LRH-1 with ligands-antagonists are indicated. *C* and *D*, mutations in the LRH-1 ligand-binding pocket (A349F and A349W, shown in *magenta* and *pink*) predicted to interfere with binding of compounds 3 and 3d2 to the receptor (shown in *C* and *D*, respectively); these mutants were used as negative controls in *in vitro* direct binding assays.

TABLE 1
Candidate compounds selected from the molecular docking screen

#	Structure	Manufacturer ID	MW[a]	Rank[b]
1	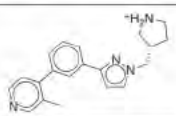	ChemBridge 28294169	319	425
2	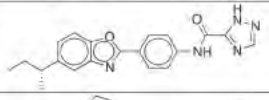	ChemBridge 7826747	361	571
3	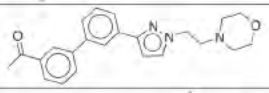	ChemBridge 94676120	375	16
4	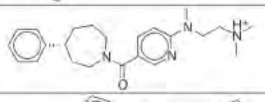	ChemBridge 66460016	382	377
5	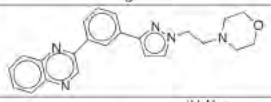	ChemBridge 55609241	385	362
6	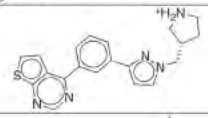	ChemBridge 99725890	362	73
7	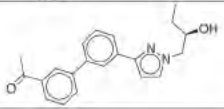	ChemBridge 58969025	334	365
8	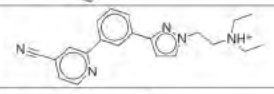	ChemBridge 96165715	346	821

[a] MW is molecular weight.
[b] Ranking of the compound in the virtual screen.

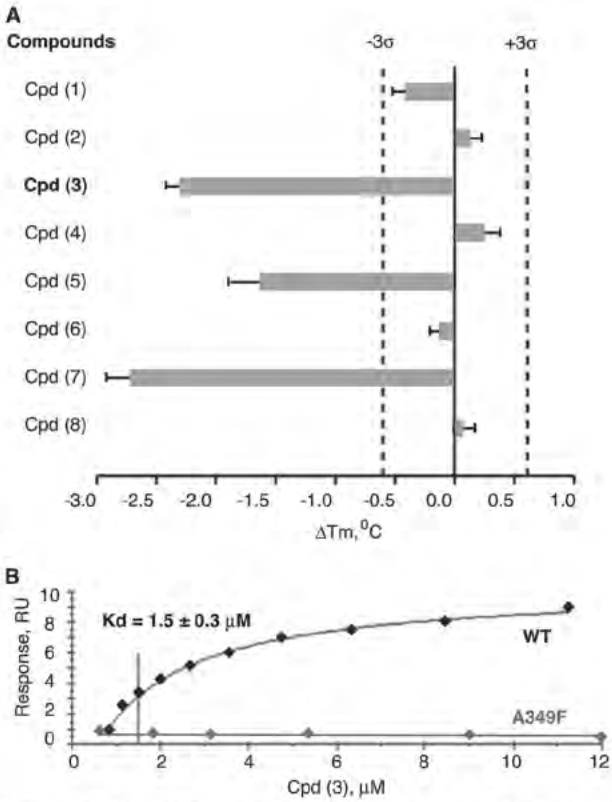

FIGURE 3. **Results of direct binding assays for eight selected LRH-1 ligands with predicted antagonistic properties.** *A*, melting temperature shifts for LRH-1 LBD treated with candidate compounds. Three out of eight receptor antagonist candidates (compounds 3, 5, and 7) shift the melting temperature (T_m) of hLRH-1 LBD, demonstrating direct binding to the receptor. For each tested compound, averaged data are shown as *horizontal bars*; experimental errors and 3σ thresholds are indicated with *solid* and *dashed lines*. Compound 3 demonstrating antagonistic effect in transcription assay is indicated in *boldface*. *B*, evaluation of binding affinity of compound 3 in Biacore-based assay. The purified LRH-1 protein (either wild type or mutant variants A349F/W) was covalently immobilized to the surface of a CM5 chip, solutions of compound 3 at 0.8–15 μM concentrations were injected over immobilized LRH-1 and reference surfaces, and dose-dependent steady-state responses were recorded and measured relative to the reference. The equilibrium dissociation constant (K_d, indicated for wild type LRH-1 LBD) was determined using steady-state analysis of binding affinities, assuming 1:1 ligand-protein stoichiometry. No dose-dependent binding was observed for LRH-1 ligand pocket mutant A349F under similar conditions (negative control, indicated).

ality of the hLRH-1 LBD was confirmed using quantitative SPR method, to measure binding and release of the receptor's co-regulator peptide. This analysis showed that a co-regulator peptide DAX1–3 ^{140}PRQGSILYSLLTSSK^{154}, which corresponds to the nuclear receptor box 3 motif of nuclear receptor DAX1, binds to hLRH-1 LBD with high affinity (K_d = 90 ± 1 nM), attesting to the DSF-based evidence of the proper receptor LBD folding; the latter is necessary to maintain a proper architecture of the receptor co-regulator binding site (AF-2), which is targeted by the DAX1–3 peptide.

When tested in the DSF experiments, three out of the eight candidate receptor antagonists (compounds 3, 5, and 7, purchased from the ChemBridge library and used at 100 μM in DSF assay) were able to shift the hLRH-1 LBD transition temperature (T_m) significantly. In the presence of compounds 3, 5, and 7, the hLRH-1 LBD T_m was 51.1 ± 0.1 °C, 51.8 ± 0.3 °C, and 50.6 ± 0.2 °C, respectively (Fig. 3*A*); no nonspecific interactions between

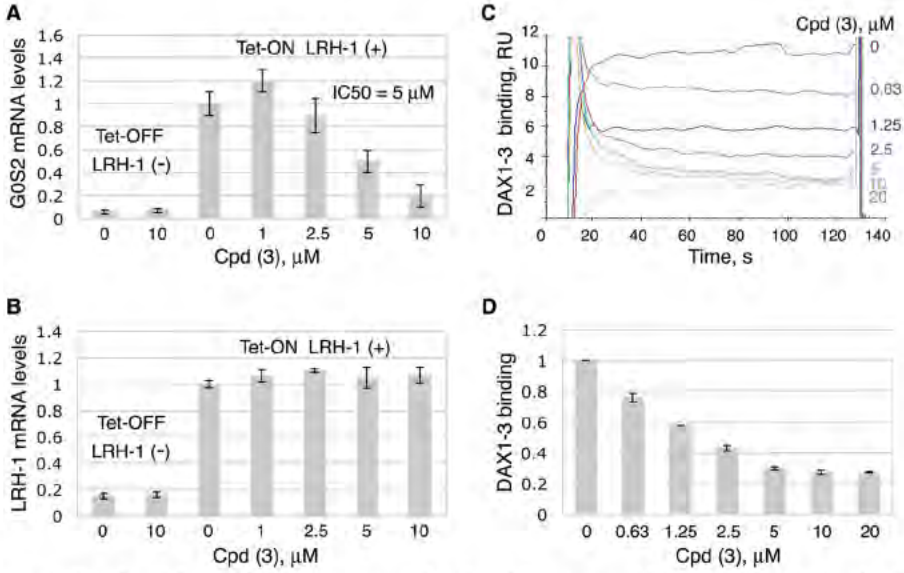

FIGURE 4. **Inhibition of transcriptional activity of LRH-1 by compound 3.** *A* and *B*, compound 3 inhibits transcriptional activity of LRH-1. HEK293 cells harboring Tet-inducible expression vector encoding full-length LRH-1 were treated with either DMSO (0.1%, solvent control) or compound 3 at different concentrations (indicated). The experiments were performed both in the presence and the absence of Tet (indicated as Tet-On LRH-1(+) and Tet-Off LRH-1(−) in *A* and *B*). Following 24-h treatments, levels of mRNA for *G0S2* (LRH-1 target gene, shown in *A*) and mRNA for LRH-1 (shown in *B*) in all cell samples were evaluated by qPCR. For each concentration point, data are shown relative to control (0.1% DMSO), as average of three independent measurements, with experimental errors shown as *black lines*. The corresponding IC_{50} value was calculated using Prism 5 software and is indicated in *A*. *C* and *D*, compound 3 diminishes binding of DAX1–3 peptide to LRH-1 in Biacore-based assay. The purified LRH-1 LBD protein was covalently immobilized to the surface of a CM5 chip, and solutions of DAX1–3 peptide at 100 nM concentration were injected over immobilized LRH-1 and reference surfaces in the presence of either 5% DMSO (solvent control) or different concentrations (0.063–40 μM) of Cpd 3. Dose-dependent steady-state responses were recorded and measured relative to the reference (shown in *C*). Quantification of the Biacore data is shown in *D*; *gray bars* indicate binding of DAX1–3 peptide in the presence of different concentrations of Cpd 3 relative to control; experimental errors are shown as *black lines*. *RU*, response units.

the compounds and the fluorescent dye were detected. Notably, all three compounds shifted the receptor T_m downward, indicating that the LRH-1 LBD is destabilized upon binding of these ligands (Fig. 3*A*; all DSF-based analyses were performed using freshly purified protein; measurements were taken in triplicates and repeated for three different batches of the protein). The observed downward shift of T_m could be explained by the presumed mode of binding of the tested compounds. The preceding molecular docking experiments predicted that binding of these molecules into the hLRH-1 ligand-binding pocket would cause detachment of helix H12 from the LBD core (Figs. 1 and 2), resulting in receptor destabilization and deactivation.

Compound 3 Inhibits Transcriptional Activity of hLRH-1—To verify that these ligands not only bind to LRH-1 but also deactivate the receptor upon binding, the transcriptional activity of LRH-1 was assessed in the absence and the presence of compounds 3, 5, and 7. HEK 293 cells expressing Tet-inducible hLRH-1 were employed to detect effects of the ligands on the receptor activity; this cellular system has been designed and used previously for assessment of transcriptional activity of nuclear receptors LRH-1 and SF-1 in the presence of synthetic small molecule agonists (32). Following the induction of LRH-1 expression with tetracycline (Tet-On LRH-1(+) in Fig. 4*A*) and treatments of HEK293 cells with either individual compounds or DMSO (0.1%, solvent control), the mRNA levels for the endogenous *G0S2* gene (G_0/G_1 switch gene, a transcriptional target of LRH-1 (32)) were evaluated in the compound-treated cells relative to the control. In these experiments, only compound 3 (1-(3′-{1-[2-(4-morpholinyl)ethyl]-1*H*-pyrazol-3-yl}-3-biphenylyl)ethanone; ranked number 16 in the preceding molecular docking screen, Table 1) inhibited the transcriptional activity of hLRH-1. Treatments with this compound lowered the *G0S2* mRNA levels with an IC_{50} value of 5 ± 1 μM (Fig. 4*A*). No changes in the levels of LRH-1 mRNA were observed as a result of these treatments (Tet-On LRH-1(+), Fig. 4*B*). Neither compound 5 nor 7 displayed any antagonist activity in these transcriptional studies (data not shown). To prove that the observed transcriptional effect by compound 3 is LRH-1-mediated, the analogous experiment was performed in noninduced HEK293 cells; under these conditions, no changes in the levels of *G0S2* transcripts were detected in cells treated with compound 3 compared with the control (Fig. 4*A*, Tet-Off LRH-1(−)). All measurements were taken in triplicates and repeated in three independent experiments.

Assessment of Binding Affinity of Compound 3—The affinity of binding interactions between compound 3 and LRH-1 LBD was determined by employing the quantitative SPR method. For this analysis, the purified LRH-1 protein (either wild type LBD or the ligand pocket mutants A349F/A349W) was covalently immobilized to the surface of a CM5 biosensor chip (for details, see "Experimental Procedures"), and solutions of compound 3 at concentrations ranging from 0.8 to 15 μM were injected over immobilized LRH-1 and reference surfaces. Compound 3 was shown to bind to wild type LRH-1 LBD, producing a steady-state SPR response in a dose-dependent manner. Curve-fitting analysis of the SPR response isotherm estimated a K_d value of 1.5 ± 0.3 μM (Fig. 3*B*). No dose-dependent binding was observed for LRH-1 ligand pocket mutants A349F and A349W under similar conditions (shown for A349F in Fig. 3*B*). These mutants were prepared based on the structure of LRH-1

TABLE 2
Structures of analogs of compound 3

#	Structure	Manufacturer ID	MW[a]
3d1	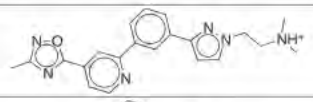	ChemBridge 18094842	375
3d2	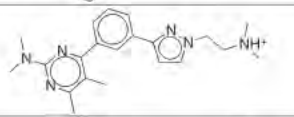	ChemBridge 16728690	365
3d3	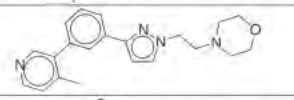	ChemBridge 75097048	348
3d4	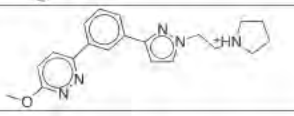	ChemBridge 56181596	350

[a] MW is molecular weight.

with the docked candidate antagonists (Fig. 2) and used as a negative control in these experiments, as the bulky amino acid substitutions in the receptor's pocket were expected to interfere with the predicted mode of ligand binding (Fig. 2, *C* and *D*). Prior to testing the mutant proteins in direct binding assays, their proper fold and stability were assessed by the DSF; no change in the transition temperature was detected for either protein variant compared with wild type LRH-1 LBD.

Further SPR analyses revealed that binding of compound 3 to LRH-1 LBD diminishes the receptor's interactions with co-regulator DAX1–3 peptide in a dose-dependent manner (Fig. 4, *C* and *D*). Being consistent with the results of transcriptional studies (Fig. 4, *A* and *B*), this observation substantiates the expected mechanism of receptor deactivation as a result of its binding to the proposed antagonist.

Selection of Compound 3 Analogs—Encouraged by the results of direct binding and transcriptional studies, we evaluated a series of commercially available analogs of compound 3 by docking them into the previously described model of LRH-1 (Fig. 1). Following these experiments, four additional top-ranked compounds with predicted receptor-specific antagonistic properties (Table 2) were purchased and analyzed in the DSF and transcriptional assays described above. The DSF studies demonstrated that one of the four candidate ligands (compound (3d2), 4-(3-{1-[2-(dimethylamino)ethyl]-1*H*-pyrazol-3-yl}phenyl)-*N*,*N*-5,6-tetramethyl-2-pyrimidinamine) shifted the transition temperature of the LRH-1 LBD significantly (from 53.4 ± 0.1 °C to 51.4 ± 0.1 °C, see Fig. 5*A*). Similar to the original compound 3, binding of this analog to hLRH-1 resulted in receptor destabilization, likely due to the detachment of helix H12 from the LBD core. This destabilization model was predicted by the molecular docking experiments (Fig. 2, *A* and *B*). All DSF measurements were taken in triplicates, using three different batches of freshly purified hLRH-1 LBD protein; no nonspecific interactions between any of the compound analogs and the fluorescent dye were detected in these experiments. Direct binding of analog (3d2) to LRH-1 has been confirmed using quantitative Biacore-based analysis. For wild type receptor, the equilibrium response data fit well to a simple 1:1 protein-ligand isotherm, with an estimated K_d value of 1.8 ± 0.4 μM (Fig. 5*B*). Under similar conditions, no binding was detected for the receptor ligand pocket mutants A349F and A349W (negative control, shown for A349F in Fig. 5*B*). Similar to compound 3 and consistent with the proposed mechanism of allosteric regulation, binding of this analog to wild type LRH-1 LBD inhibited the receptor's interactions with co-regulator DAX1–3 peptide (Fig. 6, *A* and *B*).

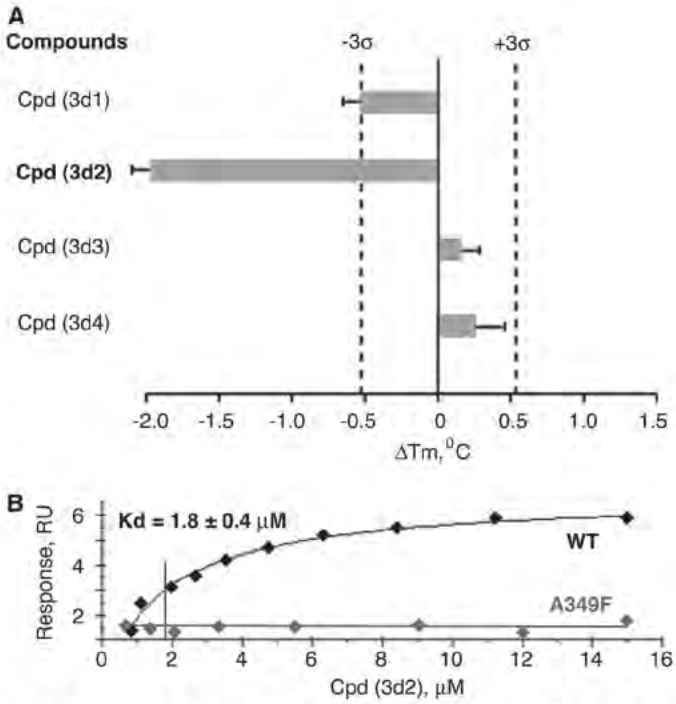

FIGURE 5. **Results of direct binding assays for selected analogs of compound 3.** *A*, melting temperature shifts for LRH-1 LBD treated with analog compounds. One out of four selected compound analogs (compound 3d2) shifts the melting temperature (T_m) of hLRH-1 LBD, demonstrating direct binding to the receptor. For each tested compound, averaged data are shown as *horizontal bars*; experimental errors and 3σ thresholds are indicated with *solid* and *dashed lines*. Analog 3d2 demonstrating antagonistic effect in transcription assay is indicated in *boldface*. *B*, assessment of binding affinity of analog 3d2 in Biacore-based analysis. The purified LRH-1 protein (either wild type or mutant variants A349F/W) was covalently immobilized to the surface of a CM5 chip; solutions of compound 3d2 at 0.8–15 μM concentrations were injected over immobilized LRH-1 and reference surfaces, and dose-dependent steady-state responses were recorded and measured relative to the reference. The equilibrium dissociation constant (K_d, indicated for wild type LRH-1 LBD) was determined using steady-state analysis of binding affinities, assuming 1:1 ligand-protein stoichiometry. Under similar conditions, no binding was observed for LRH-1 ligand pocket mutant A349F (negative control, indicated).

Following direct binding assessments by the DSF and SPR methods, the potential of compound 3d2 to inhibit transcriptional activity of hLRH-1 was evaluated using the Tet-inducible HEK293 cellular model described above. These experiments demonstrated that compound 3d2 suppresses the transcriptional activity of hLRH-1, lowering the *G0S2* mRNA levels in the treated cells compared with the control, with an IC_{50} of 6 ± 1 μM (Tet-On LRH-1(+), Fig. 6*C*). No changes in the levels of the receptor mRNA were observed as a result of these treatments (Tet-On LRH-1(+), Fig. 6*D*). Similar to the original compound 3, this analog did not exhibit any LRH-1 independent activity at or under 10 μM (Tet-Off LRH-1(−), Fig. 6*C*).

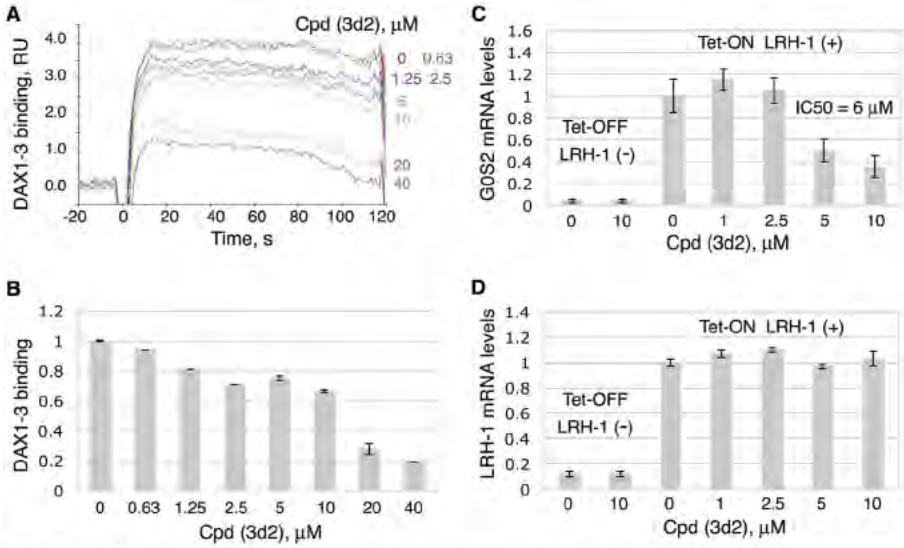

FIGURE 6. **Inhibition of transcriptional activity of LRH-1 by compound 3d2.** *A* and *B*, compound 3d2 diminishes binding of DAX1–3 peptide to LRH-1 in Biacore-based assay. The purified LRH-1 LBD protein was covalently immobilized to the surface of a CM5 chip, and solutions of DAX1–3 peptide at 100 nM concentration were injected over immobilized LRH-1 and reference surfaces in the presence of either 5% DMSO (solvent control) or different concentrations (0.063–40 μM) of Cpd 3d2. Dose-dependent steady-state responses were recorded and measured relative to the reference (shown in *A*). Quantification of the Biacore data is shown in *B*; *gray bars* indicate binding of DAX1–3 peptide in the presence of different concentrations of Cpd 3d2 relative to control; experimental errors are shown as *black lines*. *C* and *D*, compound 3d2 inhibits transcriptional activity of LRH-1. HEK293 cells harboring Tet-inducible expression vector encoding full-length LRH-1 were treated with either DMSO (0.1%, solvent control) or compound 3d2 at different concentrations (indicated). The experiments were performed both in the presence and the absence of Tet (indicated as Tet-On LRH-1(+) and Tet-Off LRH-1(−) in *C* and *D*). Following 24-h treatments, levels of mRNA for G0S2 (shown in *C*) and LRH-1 (shown in *D*) in all samples were evaluated by qPCR. For each concentration point, data are shown relative to control (0.1% DMSO), as average of three independent measurements, with experimental errors shown as *black lines*. The corresponding IC_{50} value was calculated using Prism 5 software and is indicated in *C*. *RU*, response unit.

Assessing Specificity of Compounds 3 and 3d2—To investigate a possibility that the inhibition by compounds 3 and 3d2 might be caused by their colloidal particles and thus be an artifact (51), the two ligands were evaluated by DLS and counter-screened against two model enzymes, AmpC β-lactamase and cruzain, used for the assessment of this effect (52). No colloidal particles were detected for either compound at the range of concentrations (1–10 μM) used in the transcriptional and quantitative direct binding assays (Table 3). Although particles were observed for compounds 3 and 3d2 at 50-100 μM concentrations by DLS (Table 3), these resembled precipitate, which is thought not to confer inhibition (51). Furthermore, no inhibition by either molecule at concentrations up to 100 μM was detected in the counter-screen against AmpC β-lactamase (Table 3). Although modest, up to 30%, inhibition of cruzain was observed at a higher concentration of compounds (500 μM, data not shown), this was not reversed by the addition of the nonionic detergent Triton X-100. Taken together, these observations suggest that these two ligands are not promiscuous inhibitors.

Following the promiscuous inhibition tests, we examined whether compounds 3 and 3d2 exert any effects on transcriptional activities of other nuclear receptors. Using published methods described under "Experimental Procedures," transactivation by four different nuclear receptors, steroidogenic factor 1 (SF-1, a close structural and functional homolog of LRH-1) as well as more distant receptors ERα, AR, and TRβ, was assessed in the absence and the presence of these compounds (Figs. 7 and 8). For an accurate comparison between LRH-1 and SF-1, the effects of compounds on transcriptional activity of SF-1 were evaluated using a cellular model, Tet-inducible

TABLE 3

Evaluation of compounds 3 and 3d2 for artifactual inhibition due to colloidal aggregation

Results of DLS experiments are shown for different concentrations of compounds 3 and 3d2 in the absence or presence of 0.1% Triton X-100 (indicated). Results of analysis of enzymatic activity of AmpC β-lactamase (BlaAmpC) in the presence of either compound are shown relative to solvent control (DMSO).

Colloidal aggregation assay (DLS)

Compound	Concentration (μM)	Particle Size (nM)	
		No TritonX	+0.1% TritonX
3	1	No particles	-
3	10	No particles	-
3	50	70	15
3	100	70	15
3d2	1	No particles	-
3d2	10	No particles	-
3d2	50	70	5
3d2	100	70	5

Enzyme assay (AmpC β-lactamase)

Compound	Concentration (μM)	Enzyme	Enzyme activity (%)
3	100	AmpC	103
3d2	100	AmpC	103

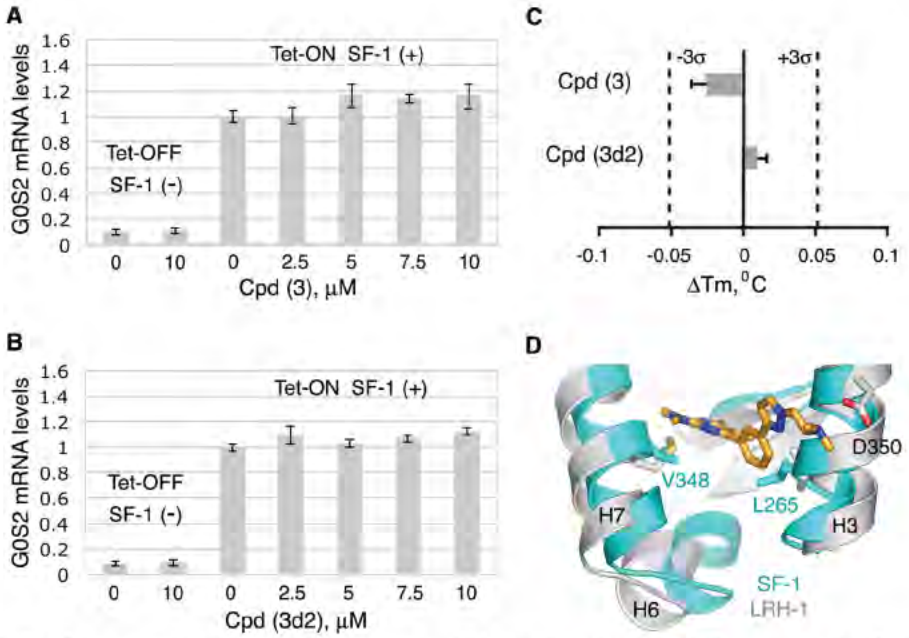

FIGURE 7. **Assessing specificity of compounds 3 and 3d2.** Neither compound 3 (*A*) nor its analog 3d2 (*B*) affect transcriptional activity of hSF-1. HEK293 cells harboring Tet-inducible expression vector encoding full-length SF-1 were treated with either DMSO (0.1%, solvent control) or individual compounds at indicated concentrations (shown in *A* for Cpd 3 and in *B* for Cpd 3d2). The experiments were performed both in the presence and the absence of Tet (indicated as Tet-On SF-1(+) and Tet-Off SF-1(−) in *A* and *B*). Following 24-h treatments, levels of mRNA for *G0S2* gene in all cell samples were evaluated by qPCR. For each concentration point, data are shown relative to control (0.1% DMSO), as average of three independent measurements, with experimental errors shown as *black lines*. *C*, melting temperature shifts for hSF-1 LBD treated with compounds 3 and 3d2. Neither compound demonstrates any significant effect on the melting temperature of the receptor. For each tested compound, averaged data are shown as *horizontal bars*; experimental errors and 3σ thresholds are indicated with *solid* and *dashed lines*. *D*, differences between hLRH-1 and hSF-1 LBPs. Selected structural elements forming the two receptors LBPs are superposed and shown in *blue* for SF-1 and in *gray* for LRH-1. Different amino acid residues in the vicinity of a docked ligand (shown for Cpd 3d2 as predicted by modeling) are indicated.

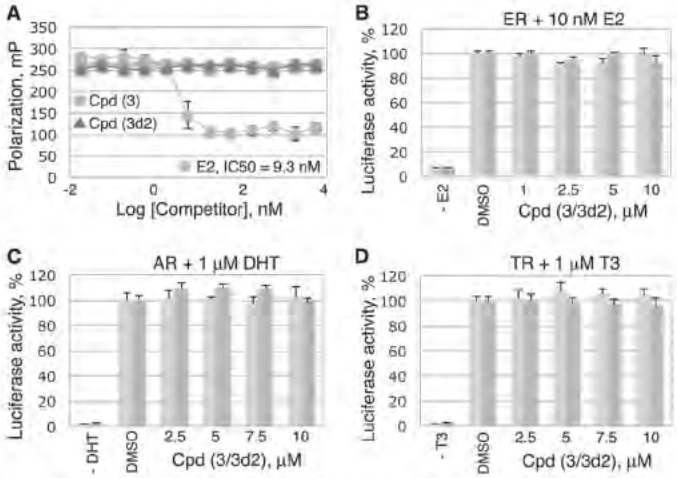

FIGURE 8. **Assessing specificity of compounds 3 and 3d2.** Neither compound 3 nor its analog 3d2 inhibits transcriptional activities of ERα, AR, or TRβ receptors. *A*, compounds 3 and 3d2 do not bind to ERα LBD in a competitive fluorescence polarization ligand binding assay. The assay was performed in a black multiwell plate using the Polarscreen™ ERα competitor assay (Invitrogen) with Fluormone™ E2-ERα complex, in the presence of either E2 (positive control) or individual compounds at different concentrations (indicated). *Error bars* indicate standard deviations from the mean values of triplicate measurements. *B*, transactivation assays with ERα in the absence or the presence of 10 nM E2 demonstrated no detectable changes in the transcriptional activity of the receptor following treatments with either Cpd 3 or Cpd 3d2 (see "Experimental Procedures" for details). *C* and *D*, analogous transactivation assays with AR and TRβ receptors (shown in *C* and *D*, see "Experimental Procedures" for details) were performed in the absence or the presence of either 1 μM dihydrotestosterone (indicated for AR in *C*) or 1 μM T3 (shown for TRβ in *D*). No detectable compound-mediated effects were observed in these experiments. *B–D*, *light* and *dark gray bars* represent data for Cpd 3 and Cpd 3d2, respectively. All measurements were done in triplicates; the corresponding data are shown as average, with experimental errors indicated.

HEK293 cells expressing SF-1 receptor, similar to that employed for the analogous experiments with LRH-1. Following the induction of SF-1 expression with tetracycline and treatments of HEK293 cells with either individual compounds or DMSO (0.1%, solvent control), the mRNA levels for the endogenous G0S2 gene (a shared transcriptional target of LRH-1 and SF-1 (32)) were evaluated in the compound-treated cells relative to the control (Fig. 7, *A* and *B*); no compound-mediated changes in the SF-1 activity were detected in these tests under similar conditions (compare Figs. 4, *A* and *B*, 6, *C* and *D*, and 7, *A* and *B*). Complementing these results, no significant shifts in melting temperature of hSF-1 LBD were recorded following treatments of the purified protein with either compound in the DSF assay (Fig. 7*C*). Combined structural differences between hLRH-1 and hSF-1 ligand-binding pockets in the vicinity of the docked ligands (shown for Cpd 3d2 model in Fig. 7*D*), might explain the discriminating binding of compounds to these receptors. In particular, more rigid Leu-265 and Val-348 residues of SF-1 (substituting for more accommodating Met-345 and Met-428 in LRH-1) could disfavor binding of the tested antagonists to SF-1.

Because selected features of the ligand-driven structural dynamics observed for ERα receptor were implemented in the model of antagonized LRH-1 LBD (Fig. 1), we tested whether the identified compounds bind to ERα. The fluorescence polarization data showed that although E2 (positive control, Fig. 8*A*) replaced a fluorescently labeled E2 bound to ERα with an estimated K_d of 9.3 nM, neither compound 3 nor 3d2 was capable of displacing the fluormone E2 ligand from ERα at concentrations

up to 10 μM. Consistent with these direct binding results, no effects of compounds on transactivation by ERα were observed in a reporter-based transcription assay (Fig. 8*B*).

Effects of the probes on transcriptional activities of two additional nuclear receptors, AR and TRβ, were analyzed in a similar luciferase reporter-based assay (Fig. 8, *C* and *D*), as described previously (46). These transcriptional studies presented no evidence of any specific probe-mediated changes in the transcriptional activities of either of the tested receptors. Based on these combined data, we conclude that the identified inhibitors bind to the LRH-1 receptor and inhibit its transcriptional activity preferentially.

Treatments with LRH-1 Antagonists Inhibit Cancer Cell Proliferation in Vitro—Because multiple LRH-1 gene targets (including *CCNE1* (encoding cyclin E1), *CCND1* (encoding cyclin D1), and c-*MYC* genes) are known to control cell growth and proliferation (7, 9), we investigated whether treatments of cells with identified receptor antagonists affect cell proliferation *in vitro*. Our previous work demonstrated that selective inhibition of LRH-1 transcription by siRNA arrests growth and proliferation of human pancreatic cancer cells (24). This receptor-mediated anti-proliferative effect was observed in four different pancreatic ductal adenocarcinoma cell lines, including AsPC-1, which express high levels of LRH-1 (24). This study shows that treatments of AsPC-1 cells with compounds 3 and 3d2 result in a similar dose-dependent inhibition of cell proliferation (Fig. 9, *A* and *B*; concentrations of compounds associated with ~50% inhibition of cell proliferation are indicated). Notably, no significant anti-proliferative effects were observed in pancreatic cancer cells L3.3 (Fig. 8, *C* and *D*) that do not express the LRH-1 receptor at a detectable level (24). In concert with these data, inhibition of transcription of LRH-1 target genes *NR0B2* and *CCNE1* (encoding SHP and cyclin E1, in *light* and *dark gray*, Fig. 9, *E* and *F*) was detected in AspC-1 but not in L3.3 cells following these treatments. No general cytotoxicity was encountered for either compound at the concentrations used for these experiments (Fig. 10, *A–D*).

We confirmed the observed anti-proliferative effects of both inhibitors in three additional human cancer cell lines known to express LRH-1: HT-29 (colon adenocarcinoma, Fig. 11, *A* and *B*) and ER-positive and -negative breast adenocarcinoma cells T47D (Fig. 11, *C* and *D*) and MDA-MB-468 (Fig. 11, *E* and *F*). Previous independent studies demonstrated that disabling of LRH-1 by either receptor-specific siRNA or genetic manipulations results in inhibition of growth and proliferation of breast (20, 21) and colon (17) cancer cells. Complementing these findings, our work reveals that proliferation rates of both breast and colon carcinoma cells are significantly compromised following treatments with LRH-1 antagonists (corresponding concentrations of compounds associated with ~50% inhibition of cell proliferation are indicated in Fig. 11, *A–F*). No significant general cytotoxicity has been detected for either compound at the tested concentration range in either cell line (Fig. 10). These results support the idea that the observed anti-proliferative effects of the probes are receptor-mediated and specific. Our data demonstrate that different types of malignant cells expressing LRH-1 are sensitive to treatments with the receptor-specific inhibitors and that growth and proliferation of LRH-1-positive cancer cells could be markedly decreased following such treatments.

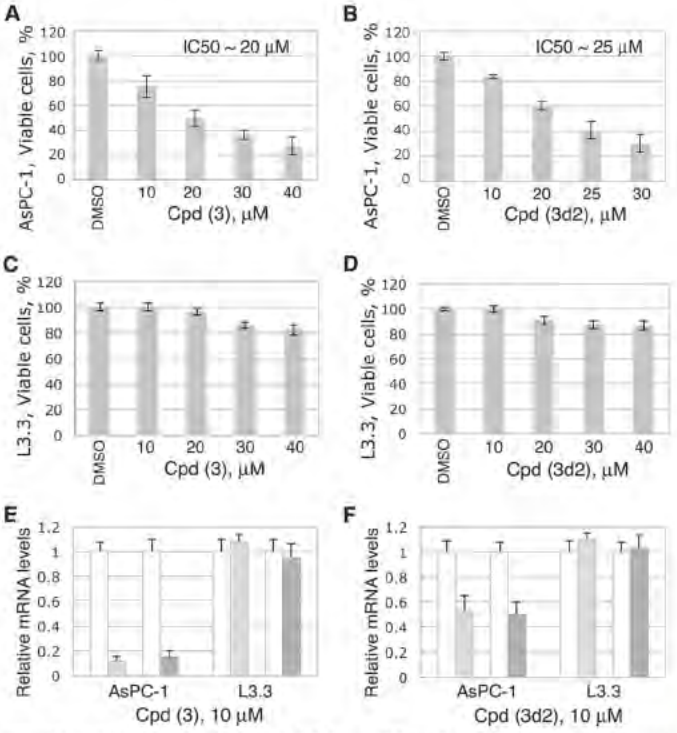

FIGURE 9. **LRH-1 antagonists inhibit proliferation of pancreatic cancer cells AsPC-1 (LRH-1-positive) but not L3.3 cells (LRH-1-negative).** *A–D*, cell proliferation rates for both pancreatic cancer cells were measured and compared in the absence and the presence of different concentrations of compounds 3 (*A* and *C*) and 3d2 (*B* and *D*) relative to control (0.1% DMSO). The corresponding IC_{50} values are indicated. Evaluations of general cytotoxic effects for both compounds in these cells were performed in parallel and are shown in Fig. 10. *E* and *F*, effects of compounds 3 (*E*) and 3d2 (*F*) on transcription of the receptor target genes *NR0B2* (encoding SHP) and *CCNE1* (encoding cyclin E1, CycE1) in AsPC-1 and L3.3 cells. Cell samples were analyzed by qPCR for the relative levels of mRNA corresponding to SHP and Cyc E1 following treatments with individual compounds at 10 μM concentration. Controls in *white* correspond to cells treated with solvent (0.1% DMSO); *light* and *dark gray bars* show the levels of mRNA for SHP and Cyc E1 in cells treated with indicated compounds. Data are shown as average of three independent measurements, with experimental errors indicated.

DISCUSSION

This work describes the identification and characterization of the first selective synthetic antagonists of human nuclear receptor LRH-1. To date, physiological hormones for this receptor have not been identified, and its regulatory mechanisms triggered by ligand binding remain largely unknown. Both synthetic and naturally occurring agonists (27–32), including phosphatidylinositol di- and triphosphates, the proposed hormone candidates (29), have been reported for this receptor. However, identification of small molecules, antagonists of LRH-1, evaded previous search efforts. We attribute the success in the discovery of LRH-1-specific inhibitors to an efficient screening strategy, which combined high throughput computer-assisted search for compounds with preferred structural characteristics with the following *in vitro* direct binding and functional assays for compound selection and validation. Such combinations of the protein-centric computational approaches with experimental verifications of the top-ranked

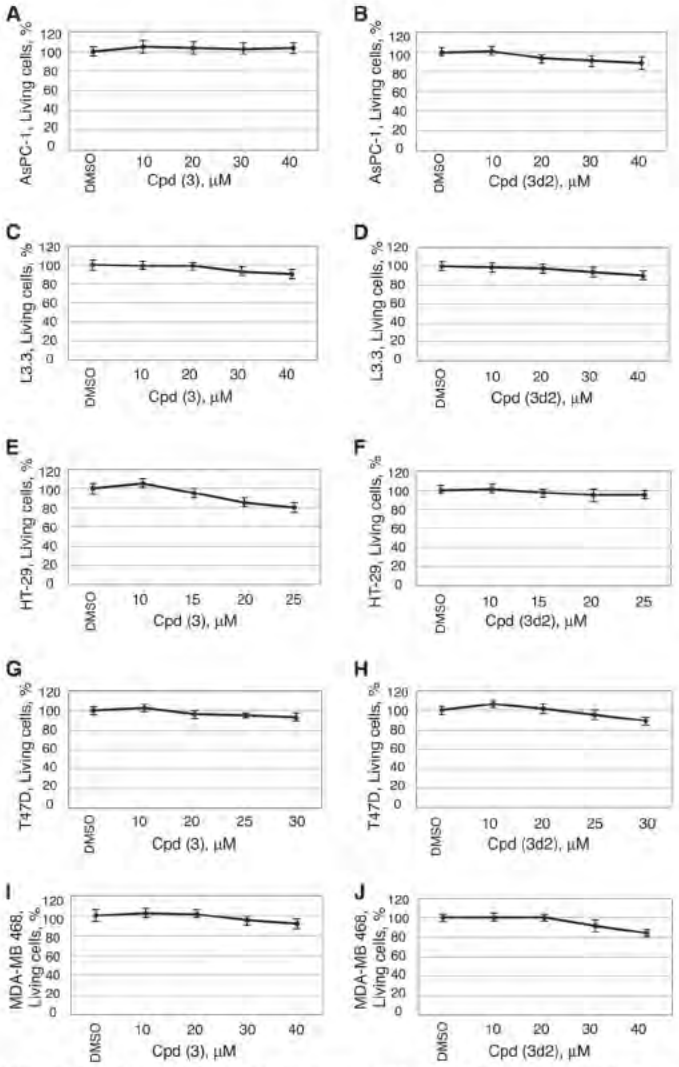

FIGURE 10. **Cytotoxicity data for human cancer cells treated with compounds 3 and 3d2.** Shown are data for pancreatic cancer cells AsPC-1 (*A* and *B*) and L3.3 (*C* and *D*), colon cancer cells HT-29 (*E* and *F*), and breast cancer cells T47D (*G* and *H*) and MDA-MB 468 (*I* and *J*). Viability measurements for cells treated with different concentrations of compounds are shown relative to control (0.1% DMSO). For each cell line, cytotoxicity was assessed 24 h following the addition of compounds, using the CytoTox-Glo cytotoxicity assay reagent (Promega). All data are shown as average of three independent measurements, and experimental errors are indicated as *black lines* (mean ± S.D.).

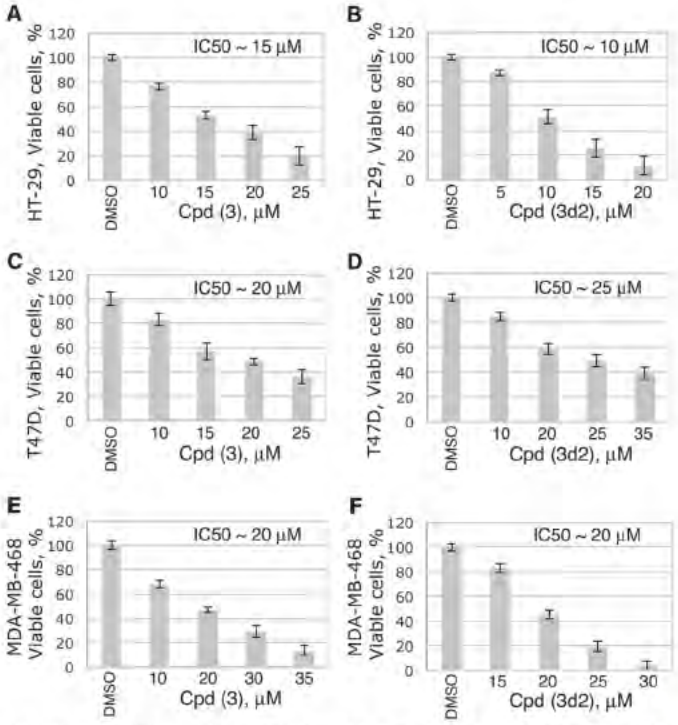

FIGURE 11. **LRH-1 antagonists inhibit proliferation of LRH-1-positive colon and breast cancer cells in a dose-dependent manner.** Cell proliferation rates for colon (*A* and *B*) as well as ER-positive (*C* and *D*) and ER-negative (*E* and *F*) breast cancer cells were measured and compared in the absence and the presence of different concentrations of compounds 3 and 3d2 relative to control (0.1% DMSO). For each cell line, concentrations of compounds associated with ~50% inhibition of cell proliferation are indicated. Evaluations of general cytotoxic effects for both compounds in these cells were performed in parallel and are shown in Fig. 10.

hits have proven to be successful for identification of specific ligands for different protein targets in the past (53–57).

A challenge that the LRH-1 target presented was the absence of a structure for the receptor in its "inactive state," which would allow docking of potential antagonists into the hormone-binding pocket. We addressed this problem by creating a model for the ligand-binding pocket of LRH-1 that would be compatible with binding of receptor-specific antagonists (Figs. 1 and 2). This model implemented structural features that facilitated binding of ligands-antagonists by human estrogen hormone receptor, for which numerous independent atomic resolution structures have been determined with different antagonists bound in the hormone-binding pocket (47–50). As a result, three out of eight candidate molecules selected for experimental verifications (compounds 3, 5, and 7, 40% of pre-selected hits, Table 1) were shown to bind to LRH-1 LBD directly, changing the melting temperature (T_m) of the protein in the DSF-based binding assay (Fig. 3). Notably, all three compounds destabilized the receptor upon binding, shifting its T_m downwards (Fig. 3, as indicated). The observed destabilizing effect was expected based on the predicted mode of binding for the presumed receptor antagonists that required undocking of helix H12 from the core LBD to facilitate their binding. Necessary exchange of phospholipids, fortuitous ligands-agonists commonly co-purified with recombinant LRH-1 LBD (29–31), for ligands-antagonists was expected to result in the receptor destabilization as well. Importantly, one of the three ligands shown to interact with the receptor directly, compound 3 (Fig. 3), compromised interactions of LRH-1 LBD with co-regulator peptide in direct binding studies (Fig. 4, *C* and *D*), most likely via distortion of the co-activator binding region of the receptor (AF-2), as was predicted by the molecular docking. Consistent with the predicted mode of binding of this ligand into the hormone-binding pocket of LRH-1, bulky amino acid substitutions in the pocket (A349F and A349W, Fig. 2*C*) abolished its binding to the receptor (shown for *A349F* in Fig. 3*B*). As expected, compound 3 also inhibited transactivation by LRH-1 in cell-based transcription assays (Fig. 4, *A* and *B*). No inhibitory effects of compound 3 on transcriptional activities of closely related and more distant receptor homologs SF-1, ERα, AR, and TRβ have been observed in these studies (Figs. 7 and 8).

Computer-assisted search for chemical analogs of compound 3 identified four additional candidate molecules (Table

2) with similar antagonistic mode of binding to the receptor (illustrated for compounds 3 and 3d2 in Fig. 2). One on these analogs, compound 3d2, was proven to bind and inhibit the transcriptional activity of LRH-1 selectively (Figs. 5–8). Similar to the original compound 3, analog 3d2 was shown to bind to the receptor's hormone pocket, destabilizing the LBD upon binding and shifting its transition temperature (T_m) downwards (Fig. 5). Furthermore, as was predicted by the molecular docking, binding of this ligand antagonized the receptor, diminishing its interactions with co-regulator peptide (shown for DAX1–3 in Fig. 6, *A* and *B*). Consequently, compound 3d2 exerted receptor-specific antagonistic effect on transcriptional activity of LRH-1 in cell-based experiments (Fig. 6, *C* and *D*). No effects on transcription by other nuclear receptors, including the closest structural and functional homolog of LRH-1, nuclear receptor SF-1 (Fig. 7), as well as ERα, AR, and TRβ (Fig. 8) were detected in these studies. These data, combined with the analogous results for the original compound 3 (Figs. 3, 4, 7, and 8, demonstrate that the identified receptor antagonists target LRH-1 preferentially. Raloxifene-based analogs were recently shown to antagonize LRH-1 (58); however, these also inhibit the ERα receptor; selectivity of these compounds for LRH-1 over SF-1 was not tested.

To confirm that the observed binding and related inhibitory effects of compounds 3 and 3d2 are not artificial (caused by their unspecific colloidal aggregation (51)), formation of colloidal particles for the identified receptor antagonists was assessed by DLS. No colloidal particles were detected for either compound at the range of concentrations (1–10 μM) used in the transcriptional and quantitative direct binding assays (Table 3). Although particles were observed for both molecules at 50-100 μM concentrations (most likely due to limited solubility and precipitation of these compounds in aqueous solutions), no unspecific inhibition by the probes at this concentration range was detected in a standard test for promiscuous inhibition (based on analysis of enzymatic activity of AmpC β-lactamase (52), Table 3). These data, combined with specificity controls used for transcription and direct binding assays (Figs. 7 and 8), show that the two LRH-1 antagonists are not promiscuous inhibitors and that their biological effects are mediated by specific target-ligand interactions.

The identification of compound 3d2 in the second round of the search elevated the success rate of our computer-assisted discovery of specific inhibitors of LRH-1 to ~17% (two novel inhibitors as a result of testing of 12 top-ranked candidates). For comparison, independent search for LRH-1 antagonists using the Prestwick Chemical Library (Illkirch, France) of 1120 drug-like chemicals, for which no computer-assisted selection of preferred candidates have been made, resulted in identification of only one compound (<0.1% of tested chemicals) capable of binding to the receptor (data not shown; all compounds were tested using the same DSF-based method for direct binding followed by the analogous transcription assay). The identified ligand was not pursued, however, as it cross-reacted with other nuclear receptors and was shown to bind to unrelated protein targets. This comparative analysis demonstrates that the success rate for an unbiased search for receptor-specific ligands approaches zero, unless a massive number of chemicals is evaluated for desired effects in high throughput experimental screenings, which require special machinery, considerable material resources, and substantial human effort (53).

In this work, the efficiency of the search for receptor antagonists was increased by incorporating a virtual computer-assisted high throughput filtering step, which 1) substantially reduced the number of compounds needed for functional analyses and 2) enriched the pool of pre-selected molecules with potential LRH-1-specific ligands. An unusual aspect of this filtering step was our use of a non-native model for the LRH-1 receptor that was based on experimental observations for the estrogen receptor. As a result, two novel LRH-1-specific antagonists have been identified in the following *in vitro* direct binding and functional assays with the input of only 12 pre-selected, top-ranked small molecules. We note that only eight candidate compounds were selected for initial experimental verifications out of 1000 top-ranked candidate molecules (see "Results"). Thus, it is plausible that more specific receptor antagonists, including those with entirely different chemotypes, could be identified if a substantially larger fraction of the candidate molecules had been tested.

The LRH-1 inhibitors identified in this work bind and antagonize receptor-mediated transcriptional activity selectively, with IC_{50} values of 5 ± 1 and 6 ± 1 μM (Figs. 4 and 6). Because no significant general cytotoxicity for these compounds is observed at these and higher concentrations (Fig. 10), these probes could be used as molecular tools for deciphering the roles of LRH-1 in different cellular contexts. For example, previous research demonstrated that selective blocking of LRH-1 function by either receptor-specific siRNA or genetic manipulations results in inhibition of growth and proliferation of cancerous cells expressing the receptor; the latter include breast (20, 21) and colon (17) cancer as well as pancreatic adenocarcinoma cells (24). The analogous, anti-proliferative effects have been observed for the epithelial cells of intestinal crypts in mice with loss-of-function mutation in the LRH-1 gene (9). The inhibitory effects are tracked to the attenuation of receptor target genes controlling cell growth, proliferation, and differentiation (9, 17, 24). Our data demonstrate that similar specific, receptor-mediated anti-proliferative effects are observed after treatments of LRH-1-positive cancer cells with the identified receptor antagonists (shown for pancreatic cancer cells in Fig. 9 and for colon and breast cancer cells in Fig. 11). We emphasize that ER-positive as well as ER-negative breast cancer cells, which both express LRH-1, are shown to be sensitive to treatments with the receptor antagonists (Fig. 11, *C–F*). These observations suggest that inhibition of LRH-1 might present a plausible route for controlling growth and proliferation of breast cancer cells that do not respond to selective estrogen receptor modulators.

Based on the results of this work, we propose that the identified LRH-1 inhibitors could be used as molecular probes for elucidating the roles of the receptor in different physiological and pathophysiological processes; in particular, they may be useful for studying developmental mechanisms as well as formation and progression of cancers of breast, colon, and pancreas. We expect that once fully characterized and optimized, LRH-1-specific antagonists could be developed into future

drugs for molecular targeted therapies of these and possibly other diseases driven by this receptor.

Acknowledgments—We thank Drs. M. McMahon, S. Gysin, and H. Ingraham for providing necessary experimental reagents; Dr. C. Filgueira for assistance with transactivation and fluorescence polarization assays for ERα receptor, and R. Villagomez for assistance with mutagenesis of LRH-1 receptor.

REFERENCES

1. Fayard, E., Auwerx, J., and Schoonjans, K. (2004) LRH-1: an orphan nuclear receptor involved in development, metabolism, and steroidogenesis. *Trends Cell Biol.* **14,** 250–260
2. Fayard, E., Schoonjans, K., Annicotte, J.-S., and Auwerx, J. (2003) Liver receptor homolog 1 controls the expression of carboxyl ester lipase. *J. Biol. Chem.* **278,** 35725–35731
3. Kim, J. W., Peng, N., Rainey, W. E., Carr, B. R., and Attia, G. R. (2004) Liver receptor homolog-1 regulates the expression of steroidogenic acute regulatory protein in human granulosa cells. *J. Clin. Endocrinol. Metab.* **89,** 3042–3047
4. Clyne, C. D., Kovacic, A., Speed, C. J., Zhou, J., Pezzi, V., and Simpson, E. R. (2004) Regulation of aromatase expression by the nuclear receptor LRH-1 in adipose tissue. *Mol. Cell. Endocrinol.* **215,** 39–44
5. Gu, P., Goodwin, B., Chung, A. C., Xu, X., Wheeler, D. A., Price, R. R., Galardi, C., Peng, L., Latour, A. M., Koller, B. H., Gossen, J., Kliewer, S. A., and Cooney, A. J. (2005) Orphan nuclear receptor LRH-1 is required to maintain Oct4 expression at the epiblast stage of embryonic development. *Mol. Cell. Biol.* **25,** 3492–3505
6. Wagner, R. T., Xu, X., Yi, F., Merrill, B. J., and Cooney, A. J. (2010) Canonical Wnt/β-catenin regulation of liver receptor homolog-1 mediates pluripotency gene expression. *Stem Cells* **28,** 1794–1804
7. Heng, J. C., Feng, B., Han, J., Jiang, J., Kraus, P., Ng, J.-H., Orlov, Y. L., Huss, M., Yang, L., Lufkin, T., Lim, B., and Ng, H.-H. (2010) The nuclear receptor Nr5a2 can replace Oct4 in the reprogramming of murine somatic cells to pluripotent cells. *Cell Stem Cell* **6,** 167–174
8. Sheela, S. G., Lee, W. C., Lin, W. W., and Chung, B. C. (2005) Zebrafish ftz-f1a (nuclear receptor 5a2) functions in skeletal muscle organization. *Dev. Biol.* **286,** 377–390
9. Botrugno, O. A., Fayard, E., Annicotte, J.-S., Haby, C., Brennan, T., Wendling, O., Tanaka, T., Kodama, T., Thomas, W., Auwerx, J., and Schoonjans, K. (2004) Synergy between LRH-1 and β-catenin induces G_1 cyclin-mediated cell proliferation. *Mol. Cell* **15,** 499–509
10. Yumoto, F., Nguyen, P., Sablin, E. P., Baxter, J. D., Webb, P., and Fletterick, R. J. (2012) Structural basis of coactivation of liver receptor homolog-1 by β-catenin. *Proc. Natl. Acad. Sci. U.S.A.* **109,** 143–148
11. Clevers, H. (2006) Wnt/β-Catenin signaling in development and disease. *Cell* **127,** 469–480
12. Villanueva, A., Newell, P., Chiang, D. Y., Friedman, S. L., and Llovet, J. M. (2007) Genomics and signaling pathways in hepatocellular carcinoma. *Semin. Liver Dis.* **27,** 55–76
13. Saif, M. W., and Chu, E. (2010) Biology of colorectal cancer. *Cancer J.* **16,** 196–201
14. Thayer, S. P., di Magliano, M. P., Heiser, P. W., Nielsen, C. M., Roberts, D. J., Lauwers, G. Y., Qi, Y. P., Gysin, S., Fernández-del Castillo, C., Yajnik, V., Antoniu, B., McMahon, M., Warshaw, A. L., and Hebrok, M. (2003) Hedgehog is an early and late mediator of pancreatic cancer tumorigenesis. *Nature* **425,** 851–856
15. Pasca di Magliano, M., Biankin, A. V., Heiser, P. W., Cano, D. A., Gutierrez, P. J., Deramaudt, T., Segara, D., Dawson, A. C., Kench, J. G., Henshall, S. M., Sutherland, R. L., Dlugosz, A., Rustgi, A. K., and Hebrok, M. (2007) Common activation of canonical Wnt signaling in pancreatic adenocarcinoma. *PLoS One* **2,** e1155
16. Takebe, N., Warren, R. Q., and Ivy, S. P. (2011) Breast cancer growth and metastasis: interplay between cancer stem cells, embryonic signaling pathways, and epithelial-to-mesenchymal transition. *Breast Cancer Res.* **13,** 211
17. Schoonjans, K., Dubuquoy, L., Mebis, J., Fayard, E., Wendling, O., Haby, C., Geboes, K., and Auwerx, J. (2005) Liver receptor homolog 1 contributes to intestinal tumor formation through effects on cell cycle and inflammation. *Proc. Natl. Acad. Sci. U.S.A.* **102,** 2058–2062
18. Sidler, D., Renzulli, P., Schnoz, C., Berger, B., Schneider-Jakob, S., Flück, C., Inderbitzin, D., Corazza, N., Candinas, D., and Brunner, T. (2011) Colon cancer cells produce immunoregulatory glucocorticoids. *Oncogene* **30,** 2411–2419
19. Wang, S. L., Zheng, D. Z., Lan, F. H., Deng, X. J., Zeng, J., Li, C. J., Wang, R., and Zhu, Z. Y. (2008) Increased expression of hLRH-1 in human gastric cancer and its implication in tumorigenesis. *Mol. Cell. Biochem.* **308,** 93–100
20. Annicotte, J. S., Chavey, C., Servant, N., Teyssier, J., Bardin, A., Licznar, A., Badia, E., Pujol, P., Vignon, F., Maudelonde, T., Lazennec, G., Cavailles, V., and Fajas, L. (2005) The nuclear receptor liver receptor homolog-1 is an estrogen receptor target gene. *Oncogene* **24,** 8167–8175
21. Thiruchelvam, P. T., Lai, C. F., Hua, H., Thomas, R. S., Hurtado, A., Hudson, W., Bayly, A. R., Kyle, F. J., Periyasamy, M., Photiou, A., Spivey, A. C., Ortlund, E. A., Whitby, R. J., Carroll, J. S., Coombes, R. C., Buluwela, L., and Ali, S. (2011) The liver receptor homolog-1 regulates estrogen receptor expression in breast cancer cells. *Breast Cancer Res. Treat.* **127,** 385–396
22. Chand, A. L., Herridge, K. A., Thompson, E. W., and Clyne, C. D. (2010) The orphan nuclear receptor LRH-1 promotes breast cancer motility and invasion. *Endocr. Relat. Cancer* **17,** 965–975
23. Dubé, C., Bergeron, F., Vaillant, M. J., Robert, N. M., Brousseau, C., and Tremblay, J. J. (2009) The nuclear receptors SF1 and LRH1 are expressed in endometrial cancer cells and regulate steroidogenic gene transcription by cooperating with AP-1 factors. *Cancer Lett.* **275,** 127–138
24. Benod, C., Vinogradova, M. V., Jouravel, N., Kim, G. E., Fletterick, R. J., and Sablin, E. P. (2011) Nuclear receptor liver receptor homolog 1 (LRH-1) regulates pancreatic cancer cell growth and proliferation. *Proc. Natl. Acad. Sci. U.S.A.* **108,** 16927–16931
25. Sonoda, J., Pei, L., and Evans, R. M. (2008) Nuclear receptors: Decoding metabolic disease. *FEBS Lett.* **582,** 2–9
26. Mataki, C., Magnier, B. C., Houten, S. M., Annicotte, J. S., Argmann, C., Thomas, C., Overmars, H., Kulik, W., Metzger, D., Auwerx, J., and Schoonjans, K. (2007) Compromised intestinal lipid absorption in mice with a liver-specific deficiency of liver receptor homolog 1. *Mol. Cell. Biol.* **27,** 8330–8339
27. Lee, J. M., Lee, Y. K., Mamrosh, J. L., Busby, S. A., Griffin, P. R., Pathak, M. C., Ortlund, E. A., and Moore, D. D. (2011) A nuclear receptor dependent phosphatidylcholine pathway with antidiabetic effects. *Nature* **474,** 506–510
28. Musille, P. M., Pathak, M. C., Lauer, J. L., Hudson, W. H., Griffin, P. R., and Ortlund, E. A. (2012) Antidiabetic phospholipid–nuclear receptor complex reveals the mechanism for phospholipid-driven gene regulation. *Nat. Struct. Mol. Biol.* **19,** 532–537
29. Krylova, I. N., Sablin, E. P., Moore, J., Xu, R. X., Waitt, G. M., MacKay, J. A., Juzumiene, D., Bynum, J. M., Madauss, K., Montana, V., Lebedeva, L., Suzawa, M., Williams, J. D., Williams, S. P., Guy, R. K., Thornton, J. W., Fletterick, R. J., Willson, T. M., and Ingraham, H. A. (2005) Structural analyses reveal phosphatidylinositols as ligands for the NR5 orphan receptors SF-1 and LRH-1. *Cell* **120,** 343–355
30. Ortlund, E. A., Lee, Y., Solomon, I. H., Hager, J. M., Safi, R., Choi, Y., Guan, Z., Tripathy, A., Raetz, C. R., McDonnell, D. P., Moore, D. D., and Redinbo, M. R. (2005) Modulation of human nuclear receptor LRH-1 activity by phospholipids and SHP. *Nat. Struct. Mol. Biol.* **12,** 357–363
31. Wang, W., Zhang, C., Marimuthu, A., Krupka, H. I., Tabrizizad, M., Shelloe, R., Mehra, U., Eng, K., Nguyen, H., Settachatgul, C., Powell, B., Milburn, M. V., and West, B. L. (2005) The crystal structures of human steroidogenic factor-1 and liver receptor homologue-1. *Proc. Natl. Acad. Sci. U.S.A.* **102,** 7505–7510
32. Whitby, R. J., Stec, J., Blind, R. D., Dixon, S., Leesnitzer, L. M., Orband-Miller, L. A., Williams, S. P., Willson, T. M., Xu, R., Zuercher, W. J., Cai, F., and Ingraham, H. A. (2011) Small molecule agonists of the orphan nuclear receptors steroidogenic factor-1 (SF-1, NR5A1) and liver receptor homolog-1 (LRH-1, NR5A2). *J. Med. Chem.* **54,** 2266–2281

33. Lee, Y. K., Choi, Y. H., Chua, S., Park, Y. J., and Moore, D. D. (2006) Phosphorylation of the hinge domain of the nuclear hormone receptor LRH-1 stimulates transactivation. *J. Biol. Chem.* **281,** 7850–7855
34. Lee, M. B., Lebedeva, L. A., Suzawa, M., Wadekar, S. A., Desclozeaux, M., and Ingraham, H. A. (2005) The DEAD-Box protein DP103 (Ddx20 or Gemin-3) represses orphan nuclear receptor activity via SUMO modification. *Mol. Cell. Biol.* **25,** 1879–1890
35. Qin, J., Gao, D. M., Jiang, Q. F., Zhou, Q., Kong, Y. Y., Wang, Y., and Xie, Y. H. (2004) Prospero-related homeobox (Prox1) is a co-repressor of human liver receptor homolog-1 and suppresses the transcription of the cholesterol 7-α-hydroxylase gene. *Mol. Endocrinol.* **18,** 2424–2439
36. Sablin, E. P., Woods, A., Krylova, I. N., Hwang, P., Ingraham, H. A., and Fletterick, R. J. (2008) The structure of co-repressor Dax-1 bound to its target nuclear receptor LRH-1. *Proc. Natl. Acad. Sci. U.S.A.* **105,** 18390–18395
37. Irwin, J. J., Shoichet, B. K., Mysinger, M. M., Huang, N., Colizzi, F., Wassam, P., and Cao, Y. (2009) Automated docking screens: a feasibility study. *J. Med. Chem.* **52,** 5712–5720
38. Mysinger, M. M., and Shoichet, B. K. (2010) Rapid context-dependent ligand desolvation in molecular docking. *J. Chem. Inf. Model.* **50,** 1561–1573
39. Lorber, D. M., and Shoichet, B. K. (1998) Flexible ligand docking using conformational ensembles. *Protein Sci.* **7,** 938–950
40. Lorber, D. M., and Shoichet, B. K. (2005) Hierarchical docking of databases of multiple ligand conformations. *Curr. Top. Med. Chem.* **5,** 739–749
41. Weiner, S. J., Kollman, P. A., Case, D. A., Singh, U. C., Ghio, C., Alagona, G., Profeta, S., and Weiner, P. (1984) A new force-field for molecular mechanical simulation of nucleic acids and proteins. *J. Am. Chem. Soc.* **106,** 765–784
42. Irwin, J. J., and Shoichet, B. K. (2005) ZINC–A free database of commercially available compounds for virtual screening. *J. Chem. Inf. Model.* **45,** 177–182
43. Li, J. B., Zhu, T. H., Cramer, C. J., and Truhlar, D. G. (1998) New class IV charge model for extracting accurate partial charges from wave functions. *J. Phys. Chem. A* **102,** 1820–1831
44. Weiner, S. J., Kollman, P. A., Nguyen, D. T., and Case, D. A. (1986) An all atom force-field for simulations of proteins and nucleic acids. *J. Comput. Chem.* **7,** 230–252
45. Wilkinson, J. M., Hayes, S., Thompson, D., Whitney, P., and Bi, K. (2008) Compound profiling using a panel of steroid hormone receptor cell-based assays. *J. Biomol. Screen.* **13,** 755–765
46. Estébanez-Perpiñá, E., Moore, J. M., Mar, E., Delgado-Rodrigues, E., Nguyen, P., Baxter, J. D., Buehrer, B. M., Webb, P., Fletterick, R. J., and Guy, R. K. (2005) The molecular mechanisms of co-activator utilization in ligand-dependent transactivation by the androgen receptor. *J. Biol. Chem.* **280,** 8060–8068
47. Shiau, A. K., Barstad, D., Loria, P. M., Cheng, L., Kushner, P. J., Agard, D. A., and Greene G. L. (1998) The structural basis of estrogen receptor/co-activator recognition and the antagonism of this interaction by tamoxifen. *Cell* **95,** 927–937
48. Brzozowski, A. M., Pike, A. C., Dauter, Z., Hubbard, R. E., Bonn, T., Engström, O., Ohman, L., Greene, G. L., Gustafsson, J. A., and Carlquist, M. (1997) Molecular basis of agonism and antagonism in the oestrogen receptor. *Nature* **389,** 753–758
49. Wu, Y. L., Yang, X., Ren, Z., McDonnell, D. P., Norris, J. D., Willson, T. M., and Greene, G. L. (2005) Structural basis for an unexpected mode of SERM-mediated ER antagonism. *Mol. Cell* **18,** 413–424
50. Pike, A. C., Brzozowski, A. M., Walton, J., Hubbard, R. E., Thorsell, A. G., Li, Y. L., Gustafsson, J. A., and Carlquist, M. (2001) Structural insights into the mode of action of a pure antiestrogen. *Structure* **9,** 145–153
51. Coan, K. E., and Shoichet, B. K. (2008) Stoichiometry and physical chemistry of promiscuous aggregate-based inhibitors. *J. Am. Chem. Soc.* **130,** 9606–9612
52. Doak, A. K., Wille, H., Prusiner, S. B., and Shoichet B. K. (2010) Colloid formation by drugs in simulated intestinal fluid. *J. Med. Chem.* **53,** 4259–4265
53. Doman, T. N., McGovern, S. L., Witherbee, B. J., Kasten, T. P., Kurumbail, R., Stallings, W. C., Connolly, D. T., and Shoichet, B. K. (2002) Molecular docking and high-throughput screening for novel inhibitors of protein tyrosine phosphatase-1B. *J. Med. Chem.* **45,** 2213–2221
54. Powers, R. A., Morandi, F., and Shoichet, B. K. (2002) Structure-based discovery of a novel, non-covalent inhibitor of AmpC β-lactamase. *Structure* **10,** 1013–1023
55. Huang, D., Lüthi, U., Kolb, P., Cecchini, M., Barberis, A., and Caflisch, A. (2006) *In silico* discovery of β-secretase inhibitors. *J. Am. Chem. Soc.* **128,** 5436–5443
56. Carlsson, J., Yoo, L., Gao, Z. G., Irwin, J. J., Shoichet, B. K., and Jacobson, K. A. (2010) Structure-based discovery of A2A adenosine receptor ligands. *J. Med. Chem.* **53,** 3748–3755
57. Schapira, M., Raaka, B. M., Das, S., Fan, L., Totrov, M., Zhou, Z., Wilson, S. R., Abagyan, R., and Samuels, H. H. (2003) Discovery of diverse thyroid hormone receptor antagonists by high-throughput docking. *Proc. Natl. Acad. Sci. U.S.A.* **100,** 7354–7359
58. Rey, J., Hu, H., Kyle, F., Lai, C. F., Buluwela, L., Coombes, R. C., Ortlund, E. A., Ali, S., Snyder, J. P., and Barrett, A. G. (2012) Discovery of a new class of liver receptor homolog-1 (LRH-1) antagonists: Virtual screening, synthesis, and biological evaluation. *ChemMedChem* **7,** 1909–1914

The signaling phospholipid PIP_3 creates a new interaction surface on the nuclear receptor SF-1

Raymond D. Blind[a], Elena P. Sablin[b], Kristopher M. Kuchenbecker[b], Hsiu-Ju Chiu[c,d], Ashley M. Deacon[c,d], Debanu Das[c,d], Robert J. Fletterick[b,1], and Holly A. Ingraham[a,1]

Departments of [a]Cellular and Molecular Pharmacology and [b]Biochemistry and Biophysics, University of California, San Francisco, CA 94158; and [c]Joint Center for Structural Genomics and [d]Stanford Synchrotron Radiation Lightsource, SLAC National Accelerator Laboratory, Menlo Park, CA 94025

Contributed by Robert J. Fletterick, September 2, 2014 (sent for review June 27, 2014; reviewed by Eric Ortlund)

The signaling phosphatidylinositol lipids PI(4,5)P_2 (PIP_2) and PI(3,4,5)P_3 (PIP_3) bind nuclear receptor 5A family (NR5As), but their regulatory mechanisms remain unknown. Here, the crystal structures of human NR5A1 (steroidogenic factor-1, SF-1) ligand binding domain (LBD) bound to PIP_2 and PIP_3 show the lipid hydrophobic tails sequestered in the hormone pocket, as predicted. However, unlike classic nuclear receptor hormones, the phosphoinositide head groups are fully solvent-exposed and complete the LBD fold by organizing the receptor architecture at the hormone pocket entrance. The highest affinity phosphoinositide ligand PIP_3 stabilizes the coactivator binding groove and increases coactivator peptide recruitment. This receptor-ligand topology defines a previously unidentified regulatory protein-lipid surface on SF-1 with the phosphoinositide head group at its nexus and poised to interact with other proteins. This surface on SF-1 coincides with the predicted binding site of the corepressor DAX-1 (dosage-sensitive sex reversal, adrenal hypoplasia critical region on chromosome X), and importantly harbors missense mutations associated with human endocrine disorders. Our data provide the structural basis for this poorly understood cluster of human SF-1 mutations and demonstrates how signaling phosphoinositides function as regulatory ligands for NR5As.

transcription | nucleus | crystallography | ligand dependent | lipid transport

The existence of nuclear, nonmembrane pools of signaling phosphorylated derivatives of phosphatidylinositols or phosphoinositides (PIP_n) was reported over two decades ago (1–3). Consistent with these early reports, lipid modifying enzymes responsible for phosphoinositide metabolism were also found in the nucleus (4–7); however, the function of PIP_n in this cellular compartment remains poorly defined. The nuclear receptors (NRs) steroidogenic factor 1 (SF-1, NR5A1) and liver receptor homolog 1 (LRH-1, NR5A2) bind phosphoinositides as well as other phospholipids in their large hydrophobic pockets (8–13). The ability of NR5As to interact with PIP_n is well conserved with the *Caenorhabditis elegans* ortholog *nhr-25* able to bind both PIP_2 and PIP_3 (14). That phosphoinositides might serve as endogenous NR5A ligands is suggested by the fact that elevating cellular pools of PIP_3 increases SF-1 activity (15) and that impairing PIP_3 uptake decreases SF-1 activity (12). Further, when purified from mammalian cells, the phosphoinositide PIP_2 is found associated with SF-1 and can be modified by the lipid kinase, IPMK, as well as the lipid phosphatase, PTEN (13). Taken together, these data suggest that signaling phosphoinositides are biologically relevant ligands for SF-1.

Phosphoinositide ligands diverge chemically from classic NR hormones in that they contain a long, extended hydrophobic moiety and a prominent hydrophilic head group, which is inherently incompatible with the hydrophobic core of the NR5A ligand binding pocket. Our previous structural analyses of SF-1 bound to phosphatidylcholine suggest that the acyl tails of phosphoinositides should be sequestered in the hydrophobic core and positioned to fill the hormone binding pockets of SF-1 and LRH-1 (11). It remains to be determined how the acyl tails and the head groups of phosphoinositides might affect the stability and activity of the NR5A ligand binding domain (LBD). To date, the only visualized phospholipid head groups in NR5As are those found in the bacterial phospholipids (bPLs), and long and medium chain phosphatidylcholines (PCs) (12, 16). Thus far, neither bPLs nor PCs complete the fold of SF-1 LBD. Indeed, in published ligand bound SF-1 structures, critical surface loops in the vicinity of the pocket entrance remain poorly ordered. This region is functionally important because it harbors disease-associated mutations in SF-1 (17–19). We hypothesized that phosphoinositide ligands with their charged head groups might anchor this site to render SF-1 fully functional.

Here, the crystal structures of SF-1 bound to PIP_2 and PIP_3 were determined, and coactivator peptide binding studies were performed to gain insights into how signaling phosphoinositides function as NR5A ligands. Based on our results, we suggest that PIP_2 and PIP_3 help organize dynamic loops in the LBD that form part of a previously unidentified regulatory surface on NR5As, similar in function to membrane bound phosphoinositides.

Results

To establish which phosphoinositide species bind SF-1 LBD with the highest affinity, stoichiometric binding to Apo SF-1 LBD was monitored in a native gel electrophoretic mobility shift assay,

Significance

We previously reported that lipids PI(4,5)P_2 (PIP_2) and PI(3,4,5)P_3 (PIP_3) bind NR5A nuclear receptors to regulate their activity. Here, the crystal structures of PIP_2 and PIP_3 bound to NR5A1 (SF-1) define a new interaction surface that is organized by the solvent-exposed PIP_n headgroups. We find that stabilization by the PIP_3 ligand propagates a signal that increases coactivator recruitment to SF-1, consistent with our earlier work showing that PIP_3 increases SF-1 activity. This newly created surface harbors a cluster of human mutations that lead to endocrine disorders, thus explaining how these puzzling mutations cripple SF-1 activity. We propose that this new surface acts as a PIP_3-regulated interface between SF-1 and coregulatory proteins, analogous to the function of membrane-bound phosphoinositides.

Author contributions: R.D.B., E.P.S., R.J.F., and H.A.I. designed research; R.D.B., E.P.S., K.M.K., H.-J.C., A.M.D., and D.D. performed research; R.D.B. contributed new reagents/analytic tools; R.D.B., E.P.S., A.M.D., D.D., and R.J.F. analyzed data; and R.D.B., E.P.S., R.J.F., and H.A.I. wrote the paper.

Reviewers included: E.O., Emory University.

The authors declare no conflict of interest.

Freely available online through the PNAS open access option.

Data deposition: The atomic coordinates and structure factors have been deposited in the Protein Data Bank, www.pdb.org [PDB ID codes 4QJR (SF-1/PIP3) and 4QK4 (SF-1/PIP2)].

[1]To whom correspondence may be addressed. Email: robert.fletterick@ucsf.edu or holly.ingraham@ucsf.edu.

This article contains supporting information online at www.pnas.org/lookup/suppl/doi:10.1073/pnas.1416740111/-/DCSupplemental.

and the apparent K_d was determined for a series of related phosphoinositides. The resulting values suggest that 3 and 5 phosphates, but not the 4 phosphate, are critical coordination points for binding SF 1 LBD. Indeed, among all dioleyl (18:1) PIP_n ligands tested, $PI(3,4,5)P_3$ and $PI(3,5)P_2$ displayed the lowest K_d values of 80 ± 12 nM and 90 ± 12 nM, respectively (Fig. 1*A* and Table S1). In comparison, affinity of RJW100 (20), a derivative of the synthetic NR5A ligand GSK8470 (21), was notably worse than $PI(3,4,5)P_3$ with an apparent K_d of 1,200 ± 270 nM, as determined here by electrophoretic mobility shift in native gels. We also noted that DLPC, a short chained exogenous phosphatidylcholine LRH 1 ligand (16, 22), binds SF 1 poorly. In conjunction with these binding assays, differential scanning fluorimetry (DSF) was used to assess the stabilizing effects of different phospholipid ligands.

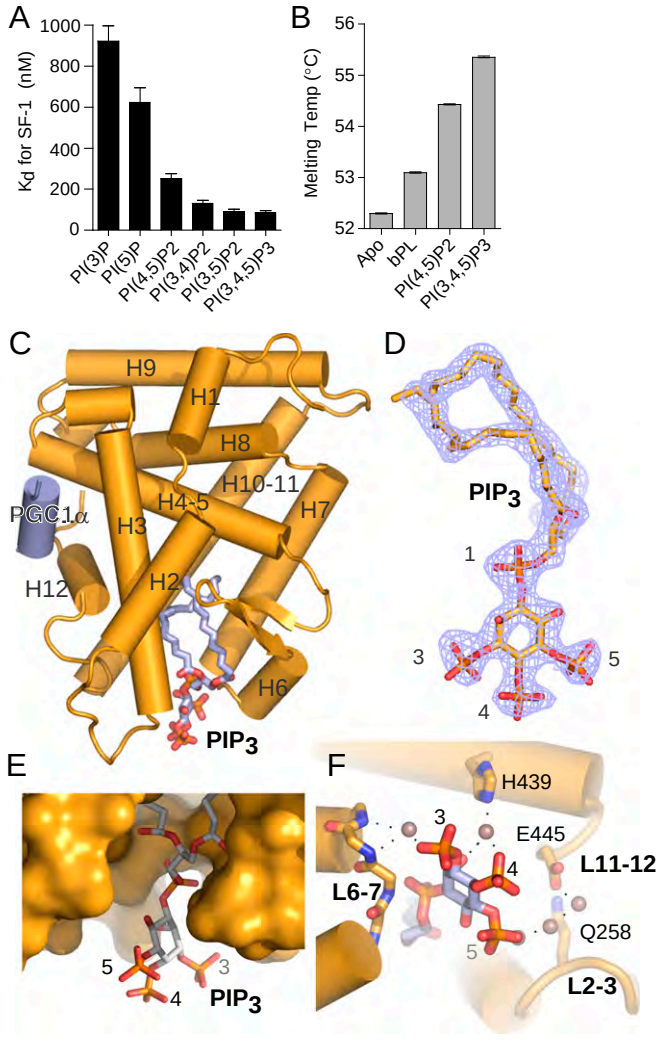

Fig. 1. Water coordination of the exposed head group in the SF 1/PIP_3 structure. (*A*) Apparent dissociation constants of indicated phosphoinositide lipids binding to the apo SF 1 LBD. (*B*) Apparent melting temperatures of SF 1 LBD in the apo (unliganded) state, complexed with copurifying bacterial phospholipid (bPL) PIP_2 or PIP_3 as determined by DSF. (*C*) Crystal structure of SF 1 LBD bound to PIP_3, PGC 1α coregulator peptide in blue, PIP_3 lipid as represented as sticks in all panels. (*D*) The final electron density map after model building and refinement ($2F_O$ F_C contoured at 1.0 σ) demonstrating unambiguous assignment of PIP_3 acyl chains and head group stereochemistry. (*E*) Surface representation of SF 1, demonstrating exposure of PIP_3 head group to solvent. (*F*) Water (indicated as copper spheres) mediated coordination of PIP_3 phosphate groups with indicated SF 1 amino acids in Loops L2 3, L6 7, and L11 12.

The melting temperatures of different ligand bound states of SF 1 LBD showed the greatest stabilization with PIP_2 and PIP_3 phosphoinositides compared with the unliganded (apo) or bacterial phospholipid (bPL) bound receptor (Fig. 1*B*); bacterial phospholipids are present in NR5As from the bacterial expression system used to produce these proteins.

The structure of SF 1 LBD bound by dipalmitoyl (C16:0, C16:0) $PI(3,4,5)P_3$ (SF 1/PIP_3) was solved by the molecular replacement method using Protein Data Bank (PDB) entry 1YOW as the search model (11) and refined to 2.40 Å with R_{free}/R_{cryst} values of 23/19% (Table S2). The structure was deposited with the PDB ID code 4QJR. SF 1/PIP_3 (Fig. 1*C*) adopts the classic NR LBD fold consisting of 12 α helices distributed in three layers with an extended helix H2 forming an additional fourth LBD layer. Similar to all other NR5A LBD structures, helix H12 assumes an active conformation, facilitating binding of PGC 1α coactivator peptide (Fig. 1*C*, blue cylinder).

The difference Fourier ($F_o - F_c$) electron density map for the SF 1 protein allowed unambiguous modeling of all elements of the dipalmitoyl (C16:0, C16:0) PIP_3 ligand (Fig. 1*D*) including the acyl chains, the bridging phosphate group at the tail to head junction, and the head group in a 1D myo configuration (Fig. S1). As expected, the bridging phosphate group of PIP_3 is coordinated and makes contacts with conserved SF 1 residues G341, Y436, and K440 (Fig. S2). Although the acyl chains of PIP_3 are shielded from the solvent in the hydrophobic hormone binding pocket, the head group of receptor bound PIP_3 is fully exposed to the solvent (Fig. 1*E*); this unique feature sets SF 1/PIP_3 apart from other protein/PIP_n structures (23 25).

Protein loops never before visualized in other published ligand bound SF 1 LBD structures are unusually well ordered in the SF 1/PIP_3 structure (Fig. S3). Because these loops are not stabilized by any direct crystal contacts, we attribute this enhanced order in the SF 1/PIP_3 structure to the presence of a highly charged solvated PIP_3 head group that forms an extensive network of water mediated interactions with the protein at the hormone pocket entrance. Stabilizing contacts involve residues in loops L2 3 (R255, D257, Q258), L6 7 (S342, L343), the C terminal portion of H11 (H439), and the following loop L11 12 (N444, E445) (Fig. 1*F*); these data confirm our earlier findings that mutating H439 (H439D) decreases PIP_3 binding to SF 1 and diminishes SF 1 activity (12).

Due to stabilizing contacts with PIP_3, the loop between helices H2 and H3 (L2 3) is imaged, to our knowledge, for the first time with a clear conformation (Fig. 2 *A* and *B*). Water molecules organized by PIP_3 stabilize side chains of R255, D257, and Q258 in L2 3, which interact directly with residues N444 and E445 in L11 12 at the base of the activation function (AF) 2 helix H12. This network of stabilizing interactions configures helix H12 for optimal interactions with transcriptional coregulators (Fig. 2*C*). Loss of function heterozygous human *NR5A1* mutations R255L, R255C, and D257N present in L2 3 are associated with human diseases, including adrenal insufficiency (17), premature ovarian failure (18), and male infertility (19). The SF 1/PIP_3 structure reveals that both of these conserved residues, R255 and D257, interact with each other and form an anchoring cluster that organizes the protein lipid surface at the entrance of the hormone pocket (Fig. 2*C*). Taken together, these data explain how *NR5A1* mutations in L2 3 cripple receptor activity (12), revealing the molecular basis of associated endocrine and reproductive disorders.

Our previous work suggests that SF 1 bound to PIP_3 is active whereas SF 1 bound to PIP_2 is less active (13). To compare these different phosphoinositide bound states, the SF 1/$PI(4,5)P_2$ structure (SF 1/PIP_2) was solved by molecular replacement, using PDB ID code 1YOW as the search model, and compared with the SF 1/PIP_3 structure (Table S2). The structure was deposited with the PDB ID code 4QK4. Superposition of the SF 1 LBD in PIP_3 and PIP_2 bound states shows that these two structures are nearly identical (Fig. 3 *A* and *B*) (rms is 0.2 Å for 256 Cα atoms).

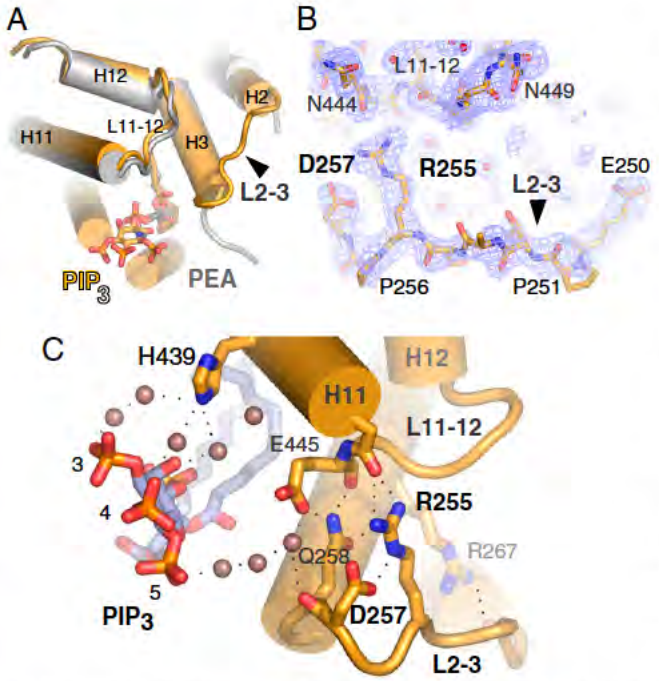

Fig. 2. PIP_3 mediated order in SF 1 loops reveals mechanism of R255 loss of function in human patients. (*A*) Current SF 1/PIP_3 structure (gold) superposed with the structure of SF 1 bound by bacterial phosphatidyl ethanolamine (gray, PDB ID code 1ZDT) (46); arrow indicates newly ordered loop between helix 2 and helix 3 (L2 3). (*B*) Electron density map ($2F_O$ F_C contoured at 1.0 σ) and stick representation of SF 1; arrow indicates newly ordered L2 3, with important residues labeled. (*C*) Water molecules (copper spheres) me diate stabilizing contacts between PIP_3 and human receptor residues R255, D257, N444, and E445. R267 stabilizes loop L2 3 at its base.

The lack of significant conformational differences between the two states could be explained by the dominant stabilizing effect of PGC1 α peptide used as a cocrystallization factor. Whereas the acyl chains of each bound ligand follow similar paths, the head group of PIP_2 is flipped relative to PIP_3 (Fig. 3*B* and Fig. S4), positioning the 5 phosphate group of PIP_2 within hydrogen bond distance from the critical H439 residue (Fig. 3*C*). These alternate conformations of the PIP_2 and PIP_3 head groups are reminiscent of the flipped orientations of the 5 phosphate of $PI(4,5)P_2$ and the 3 phosphate of $PI(3,4)P_2$ observed in the corresponding structures of the alpha tocopherol transport protein, TTPα (24); the func tional implications of these observations are unclear. The flipped orientation of the head group in the SF/PIP_2 structure might be favored by the electrostatic interaction between the 5 phosphate of PIP_2 and H439 residue (Fig. 3*C*); notably, this orientation of the head group mimics the configuration of the phosphate groups in the $PI(3,4)P_2$ that binds to SF 1 with high affinity (Table S1). Other than the flipped orientation of PIP_2 and PIP_3 head groups, all other features identified in the SF 1/PIP_2 and SF 1/PIP_3 structures were similar.

To further evaluate potential differences between SF 1/PIP_2 and SF 1/PIP_3 ligand bound states, direct binding interactions between the SF 1 LBD and coactivator PGC1 α peptide were determined by surface plasmon resonance (SPR). This method was used to ask how different ligands bound to SF 1 affect the affinity of the PGC1 α peptide and is standardly used as a read out of ligand dependent NR activation. Consistent with our observations showing the stabilizing effect of PIP_3 (Fig. 1*B*), SPR analyses show that PIP_3 induces a small, but significant, increase in SF 1 affinity for PGC 1α peptide at the AF2 site (Fig. 3*D* and Fig. S5).

The published crystal structure of mLRH 1 complexed with corepressor mDax 1 in its dimeric state shows that the second mDax 1 LBD is positioned at the NR5A hormone pocket en trance (26). Superposition of SF 1/PIP_3 and LRH 1/Dax 1 structures confirms that the PIP_3 head group and the second mDax 1 LBD are mutually exclusive as they occupy the same space (Fig. 4). In this regard, LRH 1 and SF 1 share high se quence and 3D structural homology at this site. Thus, when SF 1 is bound by PIP_3, the exposed lipid protein surface at the pocket entrance is expected to prevent the proposed repression by the Dax 1 dimer (27).

Taken together, our data demonstrate that PIP_3 is not merely a structural component of SF 1. Rather, this high affinity phos pholipid stabilizes dynamic regions at the pocket entrance, thus acting as a regulatory ligand to enhance receptor functionality through a novel protein lipid interface. These findings, coupled with our previous work linking phosphoinositide signaling to SF 1 activity, begin to demonstrate how PIPs regulate NR5As.

Discussion

Here, structural and biochemical data show that PIP_3 functions as high affinity, stabilizing ligand for SF 1. PIP_3 fills the hormone binding pocket, organizes the flexible loops at the pocket entrance, and importantly is positioned with its electrostatic head group fully exposed (Fig. 5 *A* and *B*). We posit that the solvent exposed phosphate groups of PIP_3 together with the stabilized surface

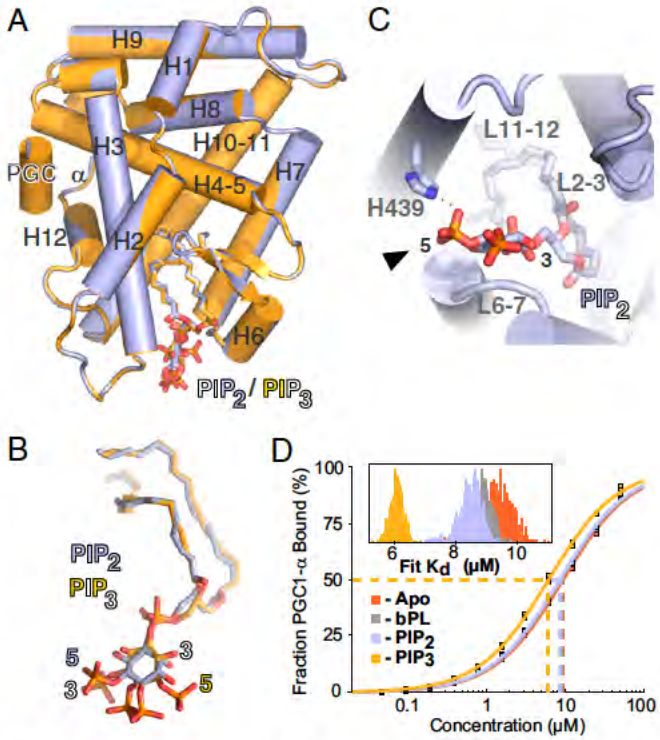

Fig. 3. SF 1/PIP_2 structure with helix 12 in the fully activated conformation. (*A*) Crystal structure of SF 1/PIP_2 (blue) superposed with SF 1/PIP_3 (gold). PGC 1α coregulator peptides are labeled and lipids are represented as sticks in all panels. (*B*) Superposition of PIP_2 and PIP_3 ligands bound to SF 1 and depicted as sticks. (*C*) Alternative view of SF 1/PIP_2, demonstrating exposure of PIP_2 head group to solvent and orientation of 5 phosphate. (*D*) Direct binding assays for four states of SF 1: bound to PIP_3, PIP_2, bPL or Apo. Relative K_d for PGC1 α peptide ±2 σ with histograms of fit K_d for four states shown in *Inset*. Mean and SD are calculated across all fits with Z scores of SF 1/PIP3 versus Apo = 4.62, bPL = 4.99, and PIP2 = 4.43 (Z statistic > 3.0 is highly significant). Binding curves with increasing concentrations of peptide are shown with dashed line indicating concentration at 50% bound ligand.

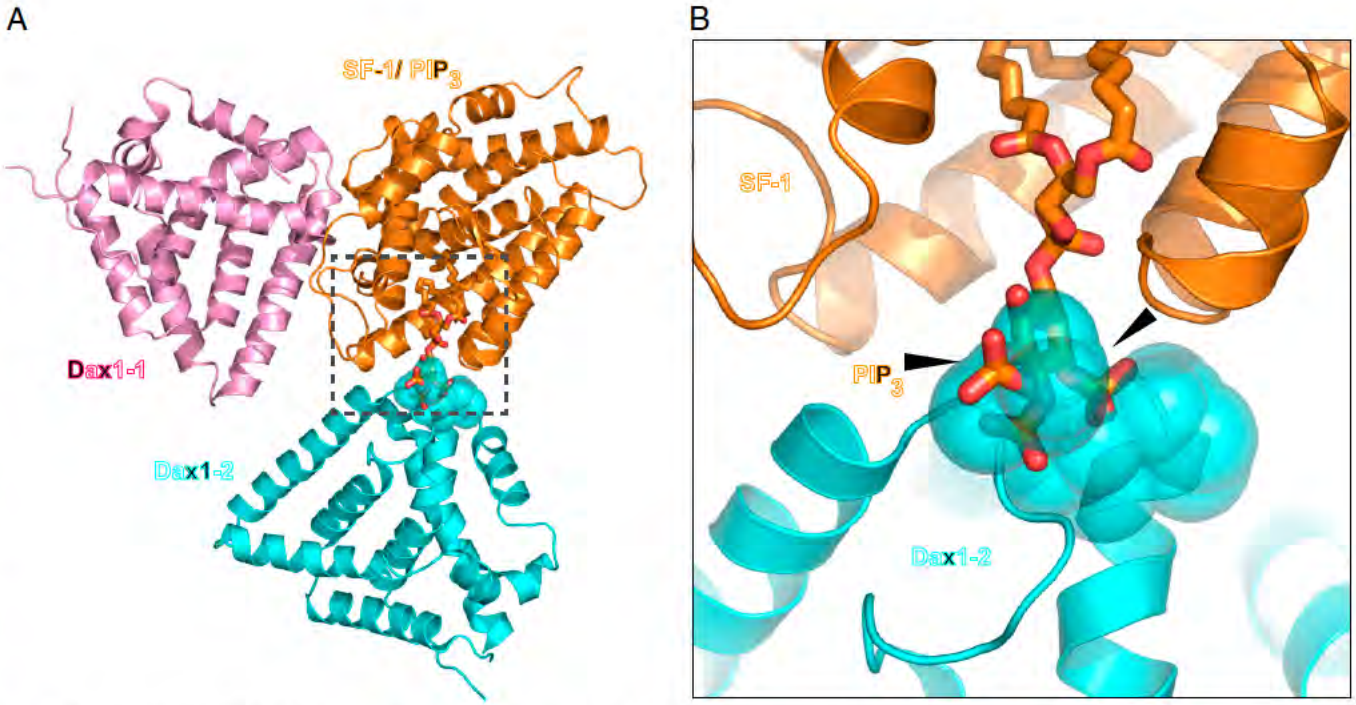

Fig. 4. PIP_3 interferes with Dax 1 corepressor interaction in simulations. (*A*) Schematic simulation of Dax1 monomer 1 (Dax1 1, pink) and monomer 2 (Dax1 2, cyan) interaction with SF 1/PIP_3 (gold), based on the LRH 1/Dax 1 crystal structure (PDB ID code 3F5C; rmsd = 0.91 Å over 237 Cα atoms). Dax1 1 interacts with the AF2 of SF 1 as expected whereas Dax1 2 interacts with a new surface on SF 1, which coincides with the PIP_3 head group. (*B*) Magnified view of the dashed box in *A*, demonstrating the steric clash between the PIP_3 head group and the Dax1 2 corepressor; arrowheads indicate points of collision. Side chains of Dax1 2 amino acids D283, Q284, and Q397 are represented as translucent cyan spheres, highlighting the coincidence.

loops function as an important regulatory site, forming a new molecular docking surface. This mechanism is analogous to the bridging functions of soluble inositols (28) or to membrane bound PIP_3 in mediating protein lipid interactions at the plasma membrane. Candidate binding partners that could dock to this nuclear protein lipid complex might include the large group of nuclear proteins shown to bind directly to phosphoinositol phosphate head groups (29) or to contain pleckstrin homology (PH) domains (30, 31). Indeed, the phosphoinositide dependent kinase 1 (PDK1) PH domain can be docked onto the SF 1/PIP_3 structure and can interface with the PIP_3 head group without any steric clashes at the solvent accessible surfaces (Fig. 5*C*). The inositol lipid kinase IPMK, previously shown to phosphorylate PIP_2 bound to SF 1, can also be docked onto the SF 1/PIP_2 structure without significant steric interference (32).

The functional significance of the opposing or "flipped" orientations of the PIP_2 and PIP_3 head groups in the SF 1 LBD structures presented here remains unclear. However, it is intriguing to note that the head groups of two phosphoinositides, $PI(3,4)P_2$ and $PI(4,5)P_2$, are also flipped in crystal structures of the TTPα lipid transport protein. Given that each position on the inositol head group has unique stereochemistry (33), one might imagine that the flipped orientations of the exposed PIP_2 and PIP_3 head groups differentially recruit stereo specific coregulators. This hypothesis is consistent with our previous data showing that, at least on a subset of SF 1 target genes, PIP_3 but not PIP_2 is required for maximal SF 1 activity (13, 15).

The new lipid protein surface created by the SF 1/PIP_n complex might also promote intramolecular domain interactions that have been observed in full length structures of the PPARγ/RXRα heterodimer (34) and the HNF4α homodimer (35) and that are proposed to form a signaling nexus that controls NR function. An important prediction to emerge from our data is that effective drug targeting of NR5As must extend beyond the receptor hydrophobic pocket. Our findings suggest that a critical regulatory site for NR5As includes the entrance to the hormone binding pocket. The 3D structures of full length SF 1 receptor in various phosphoinositide bound states should help to define the functional role of this novel lipid protein surface and might offer new strategies for developing efficient NR5A1 drugs.

Similar to phospholipid transport proteins (PLTPs) (25, 36), NR5As bury the hydrophobic tails of phosphoinositides, making the phospholipids compatible with an aqueous environment (Fig. 5*D*). The SF 1 LBD could technically be classified as a PLTP, based on its ability to exchange phospholipids between membrane systems in vitro (7, 25). However, in the few available structures of PLTPs, the phosphoinositide head groups are not accessible to solvent (24, 25, 37). In stark contrast, our SF 1/PIP_n structures establish that the PIP_n head groups have unrestricted solvent accessibility, thus allowing lipid modifying enzymes, such as IPMK and the lipid phosphatase PTEN to act on these exposed head groups (13). When considered as a PLTP that shuttles phospholipids within the nucleus, NR5As expand on that function by directly integrating lipid signaling information into a transcriptional output (Fig. 5*D*). Whether or not SF 1 acts a sensor to detect the cellular phospholipid milieu in a living cell remains to be determined. Equally intriguing is whether phosphoinositides can be loaded into SF 1 by facilitated exchange with PLTPs or by direct extraction from intracellular membranes. Clearly, it will be of great interest to determine how signaling phosphoinositides are loaded into, and decoded by, NR5As to regulate gene expression.

Materials and Methods

Protein Expression and Purification. The LBD of human SF 1 (hSF 1) was purified to homogeneity as described for mouse SF 1 LBD (12). A Cys lite version (C247S, C412S) of human SF 1 LBD was used for all crystallography. Briefly, hSF 1 LBD constructs in vector pBH4 spanning amino acids 218 461 were expressed in BL21 *Escherichia coli*, purified, and complexed with PIP_2 and

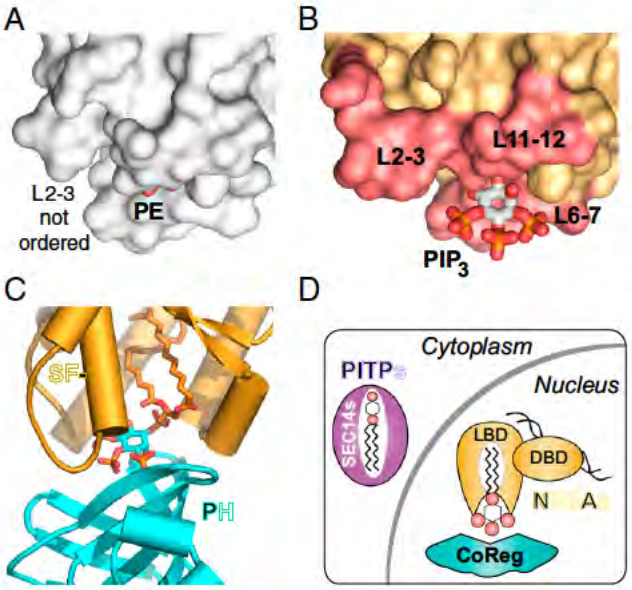

Fig. 5. PIP_3 induces a novel protein/lipid interaction surface. (*A*) Surface representation of bacterial phosphatidylethanol bound to human SF 1 LBD with the region of the disordered H2 3 indicated. (*B*) Same view as in *A*, but now PIP_3 is bound to SF 1, demonstrating ordered L2 3 and additional charges presented by the PIP_3 head group. (*C*) Docking simulation of the PH domain of PDK1 (cyan) interacting with SF 1/ PIP_3 (gold), showing possible complementarity between these two independent crystal structures. The head group (cyan) is from the PDK1 structure whereas the bridging phos phate and acyl chains are from the SF 1/PIP_3 structure. (*D*) Similar to other lipid transport proteins, SF 1 is able to resolve the conflict between the acyl chains of PIP_n and an aqueous environment. Formation of a new interaction surface used for recruiting regulatory proteins is possible when high affinity phosphatidylinositol ligands bind SF 1.

PIP_3 purchased from Cayman. PIP_2 is PI(4,5)P_2 (1,2 dipalmitoyl sn glycero 3 phospho (1′ myo inositol 4′,5′ bisphosphate, ammonium salt) and PIP_3 is PI(3,4,5)P_3 (1,2 dipalmitoyl sn glycero 3 phospho (1′ myo inositol 3′,4′,5′ trisphosphate, sodium salt), and both are fully saturated C16:0 C16:0. Ex ogenous PIP_2 or PIP_3 was added to generate SF 1/phosphoinositide complexes, as previously described (13). Protein phosphoinositide complexes were puri fied away from free phosphoinositides and bPL bound SF 1 ligand binding domain by Mono Q chromatography on an AKTA FPLC system (GE Biosciences) and concentrated for crystallization trials (15 mg/mL). A 3:1 molar excess of a peptide representing the human PGC1α cofactor (139 EEPSLLKKLLLAPA 152) was added to hSF 1/PIP_2 or hSF 1/PIP_3 complexes (15 mg/mL) in the presence of 10 μM PIP_2 or PIP_3, respectively.

Crystallization and Crystallographic Analyses of hSF 1 LBD/PIP_2 and /PIP_3. Both hSF 1/PIP_2:PGC1α and hSF 1/PIP_3:PGC1α complexes were crystallized by the vapor diffusion method, using a Mosquito (TTP Labtech), with reservoir solutions containing, respectively, 6% (vol/vol) PEG 8000, 0.2 M $Mg(OAc)_2$, and 20% (vol/vol) ethylene glycol for SF 1/PIP_2 or 10% PEG 8000, 25 mM $Mg(OAc)_2$, and 30% (vol/vol) glycerol for PIP_3 SF 1. Crystals were flash frozen in liquid nitrogen. Native data were collected at the Stanford Synchrotron Radiation Lightsource (SSRL, SLAC National Accelerator Laboratory), at 100 K, using the MicroMax 002+ Microfocus X ray generator (Rigaku) at a wavelength of 1.54 Å for SF 1/PIP_2 using a MarMosaic 325 CCD detector and beamline BL11 1 at a wavelength of 1.0 Å using a PILATUS 6M Pixel Array Detector for SF 1/PIP_3 and the BLU ICE data collection environment (38). Data were integrated and scaled using programs XDS and XSCALE (39) to 2.81 Å resolution for PIP_2 SF 1 or MOSFLM (39) and SCALA (40), imple mented in the CCP4 Program Suite (41), to 2.40 Å resolution for SF 1/PIP_3, and structure factor amplitudes were calculated using TRUNCATE (42). Both crystals were of the same space group $P4_12_12$ with cell dimensions of a = b = 75.0 Å, c = 138.6 Å (SF 1/PIP_2) and a = b = 74.9 Å, c = 139.6 Å (SF 1/PIP_3), respectively. Both crystals contained one ligand bound SF 1 complex in the asymmetric unit. The structures of both complexes were determined by the molecular replacement method using PHASER (43) as implemented in PHE NIX (44), with a search model derived from the atomic coordinates for hSF 1 (PDB ID code 1YOW) (11), with bound bacterial phospholipid and regulatory peptide omitted from the search model. Initial electron density maps were calculated from the phases of the search model. Subsequent rounds of model building and refinement were performed using the PHENIX (44) and COOT (45) programs, respectively. At later stages, both structures were checked using simulated annealing composite omit maps. All figures illus trating structural data were generated using the PyMOL molecular graphics system (Schrödinger).

DSF Stability Assays. Protein thermo stability in the presence and absence of tested phospholipids was assessed using the DSF method using the MxPro3005P qRT PCR Detection System (Stratagene) in 96 well format. Binding of Sypro Orange dye (Invitrogen) was monitored with a FAM filter for fluorescence excitation (492 nm) and a ROX filter for fluorescence emission (610 nm). The DSF spectra for purified wild type hSF 1 LBD com plexed with bacterial phospholipids PIP_2 or PIP_3 (10 μM) were recorded using a screening buffer (Tris buffered saline) with added Sypro Orange dye (1/2,000 dilution). Sample mixtures (final volume 50 μL) were heated grad ually from 25 °C to 96 °C, at the rate of 2 °C/min, and the corresponding fluorescence was recorded after every 1 °C increase. The melting tempera ture (Tm) for each sample was deduced using the KaleidaGraph program (Synergy) from the first derivative of the corresponding denaturation curve generated by the MxPro QPCR software (Stratagene). Data represent at least three independent replicates.

Surface Plasmon Resonance Coactivator Peptide Binding Assays. SPR analysis of human SF 1 LBD complexed with bPL, PIP_2, or PIP_3 was carried out on a Biacore T100 to measure the interaction between SF 1/phospholipid complexes and coregulator peptide. Matrix free surfaces were prepared by injection of Neutravidin (Invitrogen) across a planar saccharide monolayer with covalently coupled biotin (BP chips; Xantec Bioanalytics) at 15 °C in 20 mM Hepes (pH 8.0), 150 mM NaCl. Fifteen point concentration series were prepared by serial dilutions spanning 0.700 200 nM for human SF 1. Asso ciation and dissociation times were selected to ensure equilibrium and complete dissociation. All data were processed and analyzed in Matlab. Isotherms were fit to the Hill equation: fractional occupancy = $(c/(c + K_{1/2}))^{n_H}$, where c is the SF 1 concentration, $K_{1/2}$ is the SF 1 concentration producing half occupancy, and n_H is the Hill coefficient. Error in $K_{1/2}$ and n_H was determined by a bootstrap method with replacement: after scaling of n equilibrium responses for each peptide, a random set of n data points was selected with the possibility of selecting the same data point multiple times. After 1,000 iterations, the 100 best fit parameters (sum of squared errors) were used to find mean values and SD. Parameters for $t_{1/2}$ were fit from the following equations: $R = R_o\ e^{(-t \times k_{off})}$ and $t_{1/2} = \ln(2)/k_{off}$, where R = response units. Data represent at least three independent replicates.

Native Gel K_d Determinations. Apparent dissociation constants of indicated SF 1 ligands were determined on apo hSF 1 LBD by a previously described native gel shift assay to monitor equilibrium binding (13). Wild type apo hSF 1 LBD was generated by a dilution washout procedure, as follows. Human SF 1 LBD was first loaded with PIP_3 and separated from any remaining bacterial phospholipid bound SF 1 by ion exchange chromatography (Mono Q). The single SF 1/PIP_3 peak was diluted 2× with Mono Q buffer A and reloaded onto a Mono Q and washed with 1.0 L of 20 mM Hepes (8.0), 1 mM EDTA, and 2 mM CHAPS at 2 mL/min to washout PIP_3 from SF 1 LBD by dilution. The buffer was then changed into 20 mM Hepes (8.0), 1 mM EDTA to remove the CHAPS detergent, and the apo SF 1 LBD was eluted as a single peak at 11 mS/cm conductivity, allowing complete separation from any SF 1 species still retain ing PIP_3 phospholipid, which elutes as a single peak at 30 mS/cm conductivity due to the extra charge supplied by the PIP_3 head group phosphates.

All phosphoinositides used to determine apparent K_d were purchased from Avanti Polar lipids and were 1,2 dioleoyl sn glycero (C18:1, C18:1). Each phosphoinositide species was resuspended to 1 mg/mL in water, sonicated for 5 min on high power in a Branson Bioruptor bath sonicator, and then serially diluted and stored under nitrogen at 4 °C. Immediately before use, phosphoinositides were sonicated again. Two microliters of serially diluted phosphoinositide were added to binding reactions of 25 μL total volume, containing 1 μM final concentration of apo hSF 1 LBD in 20 mM Hepes (8.0), 1 mM EDTA, and 10 mM ammonium acetate in 200 μL of polypropylene PCR strip tubes. Binding reactions were incubated at 37 °C for 1 h in a PCR thermocycler with a heated reaction cover, and the reaction was mixed with 3 μL of native loading buffer [40% (vol/vol) glycerol, 0.005% Ponceau S] and run on a 4 16% polyacrylamide Bis Tris NativePage gel (Invitrogen). After fixation and silver staining (Bio Rad), gels were scanned, the phosphoinosi tide shifted band were quantitated using NIH Image, and apparent K_d was

determined by nonlinear curve fit to a single site binding model in Graph Pad Prism. RJW100 was resuspended in DMSO with the final DMSO concentration in the binding reactions to be 2.5% of the total reaction volume. Data represent at least three independent replicates.

ACKNOWLEDGMENTS. We thank Ms. T. Ruban for technical assistance in this project and Dr. C. Benod for initial guidance on the DSF, as well as members of the H.A.I. and R.J.F. laboratories and Dr. M. A. Elsliger for discussion and review of the manuscript. We also thank members of the Joint Center for Structural Genomics (JCSG) High Throughput Structural Biology pipeline for contributions to this work. Support for this project included Grants R01DK072246 and R01DK099722 (to H.A.I.), National Institute of General Medical Sciences (NIGMS) Institutional Research and Academic Career Development Awards Fellowship K12GM081266 and Grant 1K01CA172957 (to R.D.B.), Grant R01DK078075, Department of Defense Grant W81XWH 12 1 0396, and Protein Structure Initiative (PSI) Grant U01 GM094614 as part of the PSI Biology Partnership for Stem Cell Biology (to R.J.F.). The JCSG is supported by National Institutes of Health (NIH), NIGMS, Protein Structure Initiative U54 GM094586. This work was carried out as part of the PSI Biology Partnership for Stem Cell Biology. Use of the Stanford Synchrotron Radiation Lightsource (SSRL), SLAC National Accelerator Laboratory, is supported by the US Department of Energy (DOE), Office of Science, Office of Basic Energy Sciences under Contract DE AC02 76SF00515. The SSRL Structural Molecular Biology Program is supported by the DOE Office of Biological and Environmental Research and by the NIH through Grant P41 GM103393.

1. Cocco L, et al. (1987) Synthesis of polyphosphoinositides in nuclei of Friend cells. Evidence for polyphosphoinositide metabolism inside the nucleus which changes with cell differentiation. *Biochem J* 248(3):765–770.
2. Vann LR, Wooding FB, Irvine RF, Divecha N (1997) Metabolism and possible compartmentalization of inositol lipids in isolated rat-liver nuclei. *Biochem J* 327(Pt 2): 569–576.
3. Boronenkov IV, Loijens JC, Umeda M, Anderson RA (1998) Phosphoinositide signaling pathways in nuclei are associated with nuclear speckles containing pre-mRNA processing factors. *Mol Biol Cell* 9(12):3547–3560.
4. Martelli AM, et al. (1992) Nuclear localization and signalling activity of phosphoinositidase C beta in Swiss 3T3 cells. *Nature* 358(6383):242–245.
5. Divecha N, Banfić H, Irvine RF (1991) The polyphosphoinositide cycle exists in the nuclei of Swiss 3T3 cells under the control of a receptor (for IGF-I) in the plasma membrane, and stimulation of the cycle increases nuclear diacylglycerol and apparently induces translocation of protein kinase C to the nucleus. *EMBO J* 10(11): 3207–3214.
6. Shah ZH, et al. (2013) Nuclear phosphoinositides and their impact on nuclear functions. *FEBS J* 280(24):6295–6310.
7. Balla T (2013) Phosphoinositides: Tiny lipids with giant impact on cell regulation. *Physiol Rev* 93(3):1019–1137.
8. Ingraham HA, Redinbo MR (2005) Orphan nuclear receptors adopted by crystallography. *Curr Opin Struct Biol* 15(6):708–715.
9. Li Y, et al. (2005) Crystallographic identification and functional characterization of phospholipids as ligands for the orphan nuclear receptor steroidogenic factor-1. *Mol Cell* 17(4):491–502.
10. Ortlund EA, et al. (2005) Modulation of human nuclear receptor LRH-1 activity by phospholipids and SHP. *Nat Struct Mol Biol* 12(4):357–363.
11. Krylova IN, et al. (2005) Structural analyses reveal phosphatidyl inositols as ligands for the NR5 orphan receptors SF-1 and LRH-1. *Cell* 120(3):343–355.
12. Sablin EP, et al. (2009) Structure of SF-1 bound by different phospholipids: Evidence for regulatory ligands. *Mol Endocrinol* 23(1):25–34.
13. Blind RD, Suzawa M, Ingraham HA (2012) Direct modification and activation of a nuclear receptor-PIP_2 complex by the inositol lipid kinase IPMK. *Sci Signal* 5(229): ra44.
14. Mullaney BC, et al. (2010) Regulation of C. elegans fat uptake and storage by acyl-CoA synthase-3 is dependent on NR5A family nuclear hormone receptor nhr-25. *Cell Metab* 12(4):398–410.
15. Lin BC, et al. (2009) Stimulating the GPR30 estrogen receptor with a novel tamoxifen analogue activates SF-1 and promotes endometrial cell proliferation. *Cancer Res* 69(13):5415–5423.
16. Lee JM, et al. (2011) A nuclear-receptor-dependent phosphatidylcholine pathway with antidiabetic effects. *Nature* 474(7352):506–510.
17. Biason-Lauber A, Schoenle EJ (2000) Apparently normal ovarian differentiation in a prepubertal girl with transcriptionally inactive steroidogenic factor 1 (NR5A1/SF-1) and adrenocortical insufficiency. *Am J Hum Genet* 67(6):1563–1568.
18. Philibert P, et al. (2013) NR5A1 (SF-1) gene variants in a group of 26 young women with XX primary ovarian insufficiency. *Fertil Steril* 99(2):484–489.
19. Röpke A, et al. (2013) Comprehensive sequence analysis of the NR5A1 gene encoding steroidogenic factor 1 in a large group of infertile males. *Eur J Hum Genet* 21(9): 1012–1015.
20. Whitby RJ, et al. (2011) Small molecule agonists of the orphan nuclear receptors steroidogenic factor-1 (SF-1, NR5A1) and liver receptor homologue-1 (LRH-1, NR5A2). *J Med Chem* 54(7):2266–2281.
21. Whitby RJ, et al. (2006) Identification of small molecule agonists of the orphan nuclear receptors liver receptor homolog-1 and steroidogenic factor-1. *J Med Chem* 49(23):6652–6655.
22. Musille PM, et al. (2012) Antidiabetic phospholipid-nuclear receptor complex reveals the mechanism for phospholipid-driven gene regulation. *Nat Struct Mol Biol* 19(5): 532–537, S531-532.
23. de Saint-Jean M, et al. (2011) Osh4p exchanges sterols for phosphatidylinositol 4-phosphate between lipid bilayers. *J Cell Biol* 195(6):965–978.
24. Kono N, et al. (2013) Impaired α-TTP-PIPs interaction underlies familial vitamin E deficiency. *Science* 340(6136):1106–1110.
25. Schaaf G, et al. (2008) Functional anatomy of phospholipid binding and regulation of phosphoinositide homeostasis by proteins of the sec14 superfamily. *Mol Cell* 29(2): 191–206.
26. Sablin EP, et al. (2008) The structure of corepressor Dax-1 bound to its target nuclear receptor LRH-1. *Proc Natl Acad Sci USA* 105(47):18390–18395.
27. Iyer AK, Zhang YH, McCabe ER (2006) Dosage-sensitive sex reversal adrenal hypoplasia congenita critical region on the X chromosome, gene 1 (DAX1) (NR0B1) and small heterodimer partner (SHP) (NR0B2) form homodimers individually, as well as DAX1-SHP heterodimers. *Mol Endocrinol* 20(10):2326–2342.
28. Watson PJ, Fairall L, Santos GM, Schwabe JW (2012) Structure of HDAC3 bound to co-repressor and inositol tetraphosphate. *Nature* 481(7381):335–340.
29. Jungmichel S, et al. (2014) Specificity and commonality of the phosphoinositide-binding proteome analyzed by quantitative mass spectrometry. *Cell Reports* 6(3): 578–591.
30. Yu JW, et al. (2004) Genome-wide analysis of membrane targeting by S. cerevisiae pleckstrin homology domains. *Mol Cell* 13(5):677–688.
31. Lemmon MA (2004) Pleckstrin homology domains: Not just for phosphoinositides. *Biochem Soc Trans* 32(Pt 5):707–711.
32. Blind RD (2014) Disentangling biological signaling networks by dynamic coupling of signaling lipids to modifying enzymes. *Adv Biol Regul* 54:25–38.
33. Shears SB (2004) How versatile are inositol phosphate kinases? *Biochem J* 377(Pt 2): 265–280.
34. Chandra V, et al. (2008) Structure of the intact PPAR-gamma-RXR- nuclear receptor complex on DNA. *Nature* 456(7220):350–356.
35. Chandra V, et al. (2013) Multidomain integration in the structure of the HNF-4α nuclear receptor complex. *Nature* 495(7441):394–398.
36. Ren J, Schaaf G, Bankaitis VA, Ortlund EA, Pathak MC (2011) Crystallization and preliminary X-ray diffraction analysis of Sfh3, a member of the Sec14 protein superfamily. *Acta Crystallogr Sect F Struct Biol Cryst Commun* 67(Pt 10):1239–1243.
37. Tilley SJ, et al. (2004) Structure-function analysis of human [corrected] phosphatidylinositol transfer protein alpha bound to phosphatidylinositol. *Structure* 12(2): 317–326.
38. McPhillips TM, et al. (2002) Blu-Ice and the Distributed Control System: Software for data acquisition and instrument control at macromolecular crystallography beamlines. *J Synchrotron Radiat* 9(Pt 6):401–406.
39. Leslie AGW, Powell HR (2007) Processing diffraction data with Mosflm. *Evolving Methods for Macromolecular Crystallography: The Structural Path to the Understanding of the Mechanism of Action of Cbrn Agents.* Nato Science Series Series II: Mathematics, Physics, and Chemistry, eds Read RJ, Sussman J (Springer, Dordrecht, The Netherlands), Vol 245, pp 41–51.
40. Evans P (2006) Scaling and assessment of data quality. *Acta Crystallogr D Biol Crystallogr* 62(Pt 1):72–82.
41. Winn MD, et al. (2011) Overview of the CCP4 suite and current developments. *Acta Cryst* D67:235–242.
42. French S, Wilson K (1978) On the treatment of negative intensity observations. *Acta Crystallogr A* 34:517–525.
43. McCoy AJ, et al. (2007) Phaser crystallographic software. *J Appl Crystallogr* 40(4): 658–674.
44. Adams PD, et al. (2010) PHENIX: A comprehensive Python-based system for macromolecular structure solution. *Acta Crystallogr D Biol Crystallogr* 66(Pt 2):213–221.
45. Emsley P, Lohkamp B, Scott WG, Cowtan K (2010) Features and development of Coot. *Acta Crystallogr D Biol Crystallogr* 66(Pt 4):486–501.
46. Wang W, et al. (2005) The crystal structures of human steroidogenic factor-1 and liver receptor homologue-1. *Proc Natl Acad Sci USA* 102(21):7505–7510.